

**UNCLASSIFIED**

---

**AD 403 700**

*Reproduced  
by the*

**DEFENSE DOCUMENTATION CENTER**

**FOR**

**SCIENTIFIC AND TECHNICAL INFORMATION**

**CAMERON STATION, ALEXANDRIA, VIRGINIA**



---

**UNCLASSIFIED**

NOTICE: When government or other drawings, specifications or other data are used for any purpose other than in connection with a definitely related government procurement operation, the U. S. Government thereby incurs no responsibility, nor any obligation whatsoever; and the fact that the Government may have formulated, furnished, or in any way supplied the said drawings, specifications, or other data is not to be regarded by implication or otherwise as in any manner licensing the holder or any other person or corporation, or conveying any rights or permission to manufacture, use or sell any patented invention that may in any way be related thereto.

63 3 4

ASD-TDR-62-1013

403700

403 700

**INVESTIGATION OF THE GENERAL STRESS DISTRIBUTION  
IN IMPELLER WHEELS**

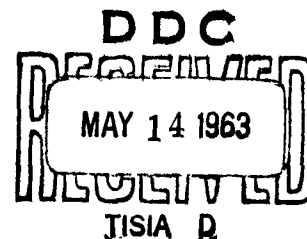
CATALOGED BY ASTIA  
AS AD NO. \_\_\_\_\_

TECHNICAL DOCUMENTARY REPORT NO. ASD-TDR-62-1013

March 1963

Directorate of Materials and Processes  
Aeronautical Systems Division  
Air Force Systems Command  
Wright-Patterson Air Force Base, Ohio

Project No. 7351, Task No. 73521



(Prepared under Contract No. AF 61(052)-520 by  
the Technische Hochschule, Aachen, Germany;  
Prof. Dr.-Ing. Wilhelm Dettmering, and Dipl.-Ing.  
Wilhelm Soetebeer, authors.)

## NOTICES

When Government drawings, specifications, or other data are used for any purpose other than in connection with a definitely related Government procurement operation, the United States Government thereby incurs no responsibility nor any obligation whatsoever; and the fact that the Government may have formulated, furnished, or in any way supplied the said drawings, specifications, or other data, is not to be regarded by implication or otherwise as in any manner licensing the holder or any other person or corporation, or conveying any rights or permission to manufacture, use, or sell any patented invention that may in any way be related thereto.

Qualified requesters may obtain copies of this report from the Armed Services Technical Information Agency, (ASTIA), Arlington Hall Station, Arlington 12, Virginia.

This report has been released to the Office of Technical Services, U.S. Department of Commerce, Washington 25, D.C., in stock quantities for sale to the general public.

Copies of this report should not be returned to the Aeronautical Systems Division unless return is required by security considerations, contractual obligations, or notice on a specific document.

## FOREWORD

This report was prepared by Institute of Turbomachines, Technische Hochschule, Aachen, Germany, under USAF Contract No. AF61(052)-520. This project was initiated under Project 7351 of Task 73521, "Stress Investigations on Impeller Wheels". The research was administered under the direction of the Directorate of Materials and Processes, Aeronautical Systems Division, Wright-Patterson Air Force Base, Ohio, with Dr. J. A. Herzog as project engineer.

The experimental work was performed during the working period from April 1961 to December 1961.

For the establishment of the tasks for the investigations as presented in this report, we are indebted to Dr. J. A. Herzog in his capacity as Project Engineer. Moreover, we wish to thank Captain D. E. Beitsch, of the European Office at Brussels, for his generous support and cooperation.

## ABSTRACT

The experimental investigations with regard to the strength of impeller wheels are intended to provide a logical supplement to calculations and to compare theoretical results with stress concentrations presently covered by the theory. While the preparatory work proceeded, which covered the conversion of the test stand for the investigation of stresses in impeller wheels as well as cementing tests for the manufacture of models and preliminary tests with regard to the application of different measuring methods, the data and program of calculation for the electronic computer were prepared. The period allowed under the present contract, which is covered by this report, was too short to enable a sufficient number of reproducible experimental investigations to be conducted which would permit a detailed comparison to be made with the calculations.

The first part of this report is a detailed description of the available calculation data for rotating shells. Efforts were made in particular to find a method of calculation which would do the fullest possible justice to the complicated geometric design of impeller wheels.


The second part of the report covers the elucidation and display of theoretical calculation results. In particular, such different influences as the number of blades, plane temperature fields, varying shell slopes etc. were examined.

The third part of the report is devoted to the description of the experimental analysis of stresses in impeller wheels. It covers a representation of the preliminary design of the model, the materials of which the models were made, the testing equipment and the initial test results. At the end of the report, reference is made to investigations that will be conducted henceforth, as well as to necessary alterations of the test stand designed to obtain higher speeds.

## PUBLICATION REVIEW

This report has been reviewed and is approved.

FOR THE COMMANDER:

  
E. M. KENNEDY, Jr., Lt. Col., USAF  
Chief, Advanced Metallurgical Studies Branch  
Metals and Ceramics Laboratory  
Directorate of Materials and Processes

## TABLE OF CONTENTS

	<u>Page</u>
Introduction . . . . .	1
I. Method for the Calculation of Stresses in Rotating Shells. 4	4
1.) Establishment of the Differential-Equations in the Theorie of Shells . . . . .	4
A) Conditions and Remarks on the Stresses to be Cal- culated . . . . .	4
B) The Differential-Equations of the Smooth Shell . 5	5
a) Establishment of the Differential-Equations of the Smooth Shell from the Equilibrium of Forces and Moments . . . . .	5
b) The Differential-Equations Derived from the Stress-Strain Relations . . . . .	6
C) Inclusion of Blades, Rings and Bores . . . . .	9
a) The Altered Design of the Differential-Equa- tions by Including the Existence of Fins . .	9
b) The Influence of Rings on the Differential- Equations . . . . .	12
c) The Influence of Additional Loads on the Differential-Equations . . . . .	16
d) The Influence of Eccentric Circular Holes upon the Differential-Equations . . . . .	17
2.) Application of the Matrix Calculus for the Determi- nation of Stresses, the Differential-Equations hav- ing been Rewritten into Equations of Differences . .	23
a) Compilation of the Differential-Equations . . .	23
b) Transformation of the Differential-Equations in- to Equations of Differences . . . . .	24
c) Application of the Matrix Calculus for Solving the Equations of Differences . . . . .	26
II. Description and Graphic Representation of Results from the Theoretical Stress Determination . . . . .	29

	<u>Page</u>
1.) Results with Impeller-Wheels whose Geometrical Shapes were Chosen Systematically . . . . .	29
2.) Theoretical Stress Distribution in the Test Models, Especially with Respect to the Influence of the Blade Number, the Poisson Ratio, and Temperature Fields . .	31
3.) Superposition of Stresses . . . . .	32
• III. Measurement of Stresses with the Rotating Model . . . . .	33
1.) Description of Model Design and Material . . . . .	33
2.) Scheme of the Test Arrangement . . . . .	34
3.) Test Procedure and Preliminary Results . . . . .	35
4.) Remarks on the Continuation of the Test Program . . . .	36
Bibliography . . . . .	37



# LIST OF FIGURES

<u>Figure</u>		<u>Page</u>
1	Stresses of an impeller wheel calculated by the method of K. J. Müller . . . . .	41
2	Specimen of a shell disaggregated into sections, with corresponding designations used in the calculations . . . .	41
3	Forces and moments acting on the shell element. The sectional areas are formed on the one hand by surface lines and on the other hand by parallel circles, and are positioned perpendicular to the medial area of shell . . . . .	42
4	Comments on the formulation of the moment through the shear stress . . . . .	43
5	Displacements of an arbitrary point on a cylindric section of the shell . . . . .	43
6	Shear deformation on the shell element for $\tau \neq \text{const}$ and $\tau = \text{const}$ . . . . .	44
7	Relation between radial stress and longitudinal stress . . .	44
8	Comments on the relation between slope and bending stress. .	45
9	Designations and forces on the finned shell element . . . .	45
10	Comments on the geometric relations for the mean length of fin $l'$ . . . . .	46
11	Illustration of the geometric dimensions and terms of a shell with fin . . . . .	46
12	Equilibrium of forces in shell and ring as well as relation between bending stresses in the shell and ring being free of longitudinal stress . . . . .	47
13	Moments on the shell element with ring zone. . . . .	47
14	Equilibrium of forces in the bore zone of shell. . . . .	48
15	Slopes and moments on a 'spoke' . . . . .	48
16	Graphic representation of the function of the meridional section of the medial shell area with different parameters $k$ to the variation of the shell contour . . . . .	49
17	Representation of possible wheel design whose contours were varied systematically . . . . .	49
18	Representation of the tangential stress $\sigma_\theta$ with varied parameters $k$ of the contour-determining function of meridional contour . . . . .	50
19	Analogous to Fig. 18, representation of the longitudinal bending stress $\sigma_l$ . . . . .	50

# LIST OF FIGURES (CONT'D)

<u>Figure</u>		<u>Page</u>
20	Analogous to Fig. 18, representation of the tangential bending stress $\sigma_p^b$ . . . . .	51
21	Analogous to Fig. 18, representation of the specified stresses $\sigma_i$ and $\tau$ . . . . .	52
22	Calculated distribution of stresses in a model wheel with different designs of the rear of wheel body . . . . .	53
23	Influence of different blade numbers on the distribution of stresses in an impeller wheel . . . . .	54
24	Influence of temperature fields on the stress fields of an impeller wheel . . . . .	55
25	Representation of assumed temperature fields with regard to the distribution of stresses according to Fig. 24 . . . . .	56
26	Superposition of the normal stress $\sigma_i$ with the bending stress $\sigma_i^b$ on a finned shell element . . . . .	56
27	Representation of the first model wheel with the principal main dimensions . . . . .	57
28	Illustration of the first built model wheel with four blades . . . . .	57
29a	General view of the test stand with model and measuring equipment . . . . .	58
29b	View of the mounted model disc in the test bed . . . . .	59
30	Representation of the way of light in a stroboscopic trans-illumination of the blades . . . . .	60
31	Measuring scheme for strain gage measuring . . . . .	60
32	Fringe pattern photo of blades of the model wheel at a speed of $n = 6000$ rpm . . . . .	61
33	Stresses determined in the symmetric section between two blades by means of strain gages . . . . .	62

# LIST OF SYMBOLS

$\sigma$	= normal stress
$\sigma_r$	= radial stress
$\sigma_l$	= longitudinal stress
$\sigma_\varphi$	= tangential stress
$\sigma_l^b$	= longitudinal bending stress
$\sigma_\varphi^b$	= tangential bending stress
$\tau$	= shear stress
$r$	= radius
$r_o$	= inner radius
$r_a$	= outer radius
$h$	= disc or shell thickness at the radius $r$
$\delta$	= angle of shell slope
$l$	= ordinate along the meridional section of the medium area of the shell
$L$	= total length of the meridional section of the medium area of the shell
$\varphi$	= angle at the center
$\gamma$	= specific weight
$g$	= gravitational constant
$P$	= force
$p$	= gas pressure
$M$	= moment
$\nu$	= Poisson ratio
$\epsilon$	= strain
$\alpha$	= linear heat extension coefficient

LIST OF SYMBOLS (CONT'D)

$\theta$	= overtemperature
$u$	= displacement
$\psi$	= alteration of angle by bending
$\phi$	= alteration of angle by shear deformation
$G$	= shear modulus
$E$	= Young's modulus
$\rho$	= radius of curvature
$s$	= centroidal distance
$w$	= moment of resistance
$V$	= volume
$F$	= area
$F$	= function
$G$	= weight
$\omega$	= angular velocity
$R$	= current resistance

## I N T R O D U C T I O N

The present Final Report entitled "Investigation of the General Stress Distribution in Impeller Wheels" cannot yet be regarded as a comprehensive study of the subject as the time spent on such investigations has been too short. The object of the work done so far has therefore been to complete the necessary preparatory work under the aspects of theory and experimental technique.

The test stand, which was formerly used for discs of uniform thickness was converted to suit the examination of impeller wheels. The model materials that offered themselves considering relatively easy workability and the advantage of joining components by a cement were the same plastic materials that had so far been used for photoelastic purposes; it was from these materials that the first plastic models were made.

Three test methods were used for the experimental stress analysis:-

1. Photo-elasticity in examining blades which, being at first of equal thickness, show a largely plane state of stresses.
2. Measurement by means of strain gages.
3. The method of brittle-coating which will be applied supplementary to the measurements with strain gages.

The design of the wheel body was first determined by the contours of the wheel surface carrying the gas flow where the contours were to be identical with the gas flow line of a plane stagnation-point function. It has meanwhile been found, however, that other aspects existed in determining the design of wheels used for stress analyses, particularly with regard to the

---

Manuscript released by the authors March 1962 as an ASD Technical Documentary Report

theoretical calculation of stresses. In particular, the subsequently selected design determining function permitted the slope of the shell to be varied through variation of only one of the parameters required for the calculation of strengths.

Experimental investigations of stresses in arbitrarily shaped impeller wheels will only reveal general information if experimentally established values are compared to calculated values which are obtained through reasonable processes of calculation and diminishing of the existing problem as far as possible. However, if practical stress concentration factors at corresponding points on wheels of various related shapes are to be established it will be found that most of the former calculation methods hardly permit a comparison with experimental results. The determination of stress distribution in wheel bodies may be based on the shell theory but such calculation does not include the stress concentration factors subject to the variation in shape of the wheel and blade. It would be going too far to specify all conceivable methods of calculation which always depart from the symmetric disk disregarding any slope of the medial area of the wheel from the vertical to the rotational axis. The simplest method of calculation may be to relate the sectional area, symmetrically to a medial area, vertically to the rotational axis, taking into account the blades either by the specific gravity /7/ of the disk as it is or as the increased thickness /30/ of the disk profile. Such methods of calculation permit the utilization of an arbitrary profile which may be calculated by the known methods of Grammel, Donath-Karas, Keller-Salzmann, Kissel, or by the method of differences.

An interesting method of calculation has been suggested by K. J. Müller /29/, which however takes into account only the nonsymmetrical design of the wheel with regard to the radial blading. The blades are assumed as removed from the disk and the displacement of the disk-disregarding any pronounced slope - and that of the blade star are considered to be separated by the centrifugal forces. Statically indeterminate forces are applied to the virtual sectional areas so as to produce an equal displacement of the disk and blades in these areas. Here again, calculation will be conditional on the simplification of an axially symmetrical loading and dilation of the complete wheel. However, to render an analytical solution of the system of general differential equations possible from an equilibrium of forces and also from a state of deformation, the method of K. J. Müller requires the actual profile contour to be approximated by a hyperbolical profile design of the term  $h = C(r/r_a)^{-8}$  with  $r_a$  being the external radius. Figure 1 shows for the example of a shell the relative stress terms which were calculated by the method of K. J. Müller. The statically indeterminate forces result in shear stresses

at the virtual sectional areas between disk and blades. Even the latter method requires a considerable calculatory effort if the statically indeterminate forces are to be determined with accuracy and only if table computers are available.

I. Method for the Calculation of Stresses in Rotating Shells and its Interpretation

1. Establishment of the Differential-Equation in the Theory of Shells

A) Conditions and Remarks on the Stresses to be Calculated

If the problem of rotating shells is to be solved more comprehensively, the greater calculatory effort involved requires the use of electronic computers. In a recently published book by K. Löffler called "The Calculation of Rotating Disks and Shells", Springer-Verlag: Berlin/Göttingen/Heidelberg 1961, a method of calculation is described which permits the entire state of stresses in rotating shells to be covered to a wide extent, which was demanded above. By this method, radial blades, cantilever rings as well as eccentric holes can be taken into account right from the beginning. One of the conditions this method requires is that the shell of revolution be resistant to bending. Its state of stresses is described by five stress terms, viz. the longitudinal stress  $\sigma_l$ , whose direction must be fixed in relation to that of a meridional section of the medial area of the shell, the tangential stress  $\sigma_\varphi$ , the longitudinal bending stress  $\sigma_l^b$ , the tangential bending stress  $\sigma_\varphi^b$  and a shear stress  $\tau$ , which is to act in the direction of the normal to the medial area of the shell and is assumed to be the mean shear stress of equal value in the whole cross section. In establishing the differential equations for the rotating shell, the simplified but largely reliable arrangement is made that  $\sigma_l$  and  $\sigma_\varphi$  are taken to be invariable within the thickness  $h$  of the shell and that the corresponding superposing bending stresses are linear over the cross section.



## B) The Differential-Equations of the Smooth Shell

### a) Establishment of the Differential-Equations of the Smooth Shell from the Equilibrium of Forces and Moments

In Figure 2 the slope refers to the inclination of the meridional section of the medial area of shell, the ordinate normal to the axis of rotation. With  $\delta = 0$  over the entire extent of the disk would be symmetric. In Figure 3 a shell element is cut out of the shell of revolution, the angle  $\delta$  being variable within the shell element.

Formulation of the equilibrium at the mere shell element without any additional fins.

The equilibrium of forces in the direction of the meridional section of the medial area of the shell results, as is shown in Figure 3, in the following differential equation:

$$d(\sigma_1 h r d\varphi) - \sigma_\varphi h d l d\varphi \cos \delta + \tau h r d\varphi d\delta + h d l r d\varphi \frac{\gamma}{g} r \omega^2 \cos \delta = 0 \quad (1)$$

A few forces which are small in the higher powers have not been recorded, which applies also to the following.

The equilibrium in the direction of the normal toward the medial area of the shell element under consideration is formulated as follows:

$$d(\tau h r d\varphi) - \sigma_\varphi h d l d\varphi \sin \delta - \sigma_1 h r d\varphi d\delta + h d l r d\varphi \frac{\gamma}{g} r \omega^2 \sin \delta + p r d\varphi d l = 0 \quad (2)$$

In the last equation (2) the letter p means the gas pressure. From the forces and bending stresses entered in Figure 3 and from the geometry of the shell element, the equilibrium of the moments existing around the tangents on a parallel circle of the medial area of the shell may now be easily read off at the upper edge of the shell element:

$$d(\sigma_r^b \frac{h^2}{6} r d\varphi) - \sigma_\varphi^b \frac{h^2}{6} dl d\varphi \cos \delta + dM_\tau = 0 \quad (3)$$

The moment by the shear stress  $\tau$  at the lower edge of shell around the previously chosen direction is expressed by the following formula wherein  $dx$  means the chord length of arc  $dl$  (see Figure 4):

$$dM_\tau = \tau h r d\varphi \cos \frac{d\delta}{2} \cdot dx \quad (4)$$

The term obtained for the length of chord is

$$dx = 2 \sin \frac{d\delta}{2} \cdot \frac{dl}{d\delta}$$

thus resulting in  $dM_\tau = \tau h r d\varphi dl \frac{2 \cos \frac{d\delta}{2} \sin \frac{d\delta}{2}}{d\delta} = \tau h r d\varphi dl \frac{\sin d\delta}{d\delta}$

The equilibrium of the moments can now be definitely expressed as follows:

$$d(\sigma_r^b \frac{h^2}{6} r d\varphi) - \sigma_\varphi^b \frac{h^2}{6} dl d\varphi \cos \delta + \tau h dl r d\varphi \frac{\sin d\delta}{d\delta} = 0 \quad (5)$$

#### b) The Differential-Equations Derived from the Stress-Strain Relations

From the equilibrium of the forces and moments three equations could be established; another two equations will have to be formulated from the state of deformation in order to arrive at the five terms that are wanted.

With regard to the displacements, Hooke's law may in general be applied to the variable stresses  $\sigma^*$  extending over the whole cross section, i.e. at first to radial stresses and strains, which may later be replaced however by the relative terms in the direction of  $l$

$$\sigma_r^* = \frac{E}{1-\nu^2} [(\epsilon_r + \nu \epsilon_\varphi) - (1+\nu)\alpha \vartheta]$$

$$\sigma_\varphi^* = \frac{E}{1-\nu^2} [(\nu \epsilon_r + \epsilon_\varphi) - (1+\nu)\alpha \vartheta] \quad (6)$$

$\alpha$  is the linear coefficient of thermal expansion and  $\vartheta$  any over-temperature. If the further terms are adopted from Figure 5,  $\psi$  represents the slope produced by bending,  $\beta$  the torsion caused by shear deformation (see Fig. 6), and  $k$  the distance between the central section line and the chosen ordinate.  $u$  is the displacement of an arbitrary point on the cylindrical section with the coordinates  $r$  and  $y$  for which  $u(r, y)$  is formulated as follows.

$$\begin{aligned} u(r, y) &= u(r) + (y-k)(\psi + \beta) \\ \varepsilon_r &= \frac{\partial u(r, y)}{\partial r} = \frac{du(r)}{dr} + (y-k) \frac{d\psi}{dr} - \psi \frac{dk}{dr} - \beta \frac{dk}{dr} + (y-k) \frac{d\beta}{dr} \\ \varepsilon_\varphi &= \frac{u(r, y)}{r} = \frac{u(r)}{r} + \frac{(y-k)}{r} \psi + \frac{(y-k)}{r} \beta \end{aligned} \quad (7)$$

The general stresses now take the formula

$$\begin{aligned} \sigma_r^* &= \frac{E}{1-\nu^2} \left[ \frac{du}{dr} + (y-k) \frac{d\psi}{dr} - \psi \frac{dk}{dr} + (y-k) \frac{d\beta}{dr} - \beta \frac{dk}{dr} + \nu \frac{u}{r} + \nu \frac{y-k}{r} (\psi + \beta) - (1+\nu)\alpha\vartheta \right] \\ \sigma_\varphi^* &= \frac{E}{1-\nu^2} \left[ \nu \frac{du}{dr} + \nu(y-k) \frac{d\psi}{dr} - \nu\psi \frac{dk}{dr} + \nu(y-k) \frac{d\beta}{dr} - \nu\beta \frac{dk}{dr} + \frac{u}{r} + \frac{y-k}{r} (\psi + \beta) - (1+\nu)\alpha\vartheta \right] \end{aligned} \quad (8)$$

The tractions  $P_r$  and  $P_\varphi$  are obtained from the integration of stresses  $\sigma_r^*$  and  $\sigma_\varphi^*$  across the cross section between the boundaries  $y_{1,2} = k \pm y_0/2$ .

The tensile stresses result from

$$\sigma_r = \frac{P_r}{2\pi r y_0} = \frac{1}{y_0} \int_{k-\frac{y_0}{2}}^{k+\frac{y_0}{2}} \sigma_r^* dy; \quad \sigma_\varphi = \frac{P_\varphi}{dr y_0} = \frac{1}{y_0} \int_{k-\frac{y_0}{2}}^{k+\frac{y_0}{2}} \sigma_\varphi^* dy \quad (9)$$

If  $dk/r$  is regarded as negligibly small, and  $dk/dr = \tan \delta$  one obtains - since an appreciable number of terms add up to zero - the stresses that are constant in the cross section:

$$\begin{aligned} \sigma_r &= \frac{E}{1-\nu^2} \left[ \frac{du}{dr} - (\psi + \beta) \tan \delta + \nu \frac{u}{r} - (1+\nu)\alpha\vartheta \right] \\ \sigma_\varphi &= \frac{E}{1-\nu^2} \left[ \nu \frac{du}{dr} - \nu (\psi + \beta) \tan \delta + \frac{u}{r} - (1+\nu)\alpha\vartheta \right] \end{aligned} \quad (10)$$

Figure 7 shows the relation between  $\sigma_l$  and  $\sigma_r$ :

$$\sigma_l = \frac{P_l}{2\pi r h} = \frac{P_r \cos \delta}{2\pi r h} = \frac{P_r}{2\pi r y_0} = \sigma_r \quad (11)$$

$h$  is the thickness of the shell at the point examined if it is measured normal to the medial area of the shell.

An examination of the bending moments at the shell element leads to the slope  $\psi$ , which we should like to have eliminated from the equations so far established. Figure 8 permits the establishment of the following relations between torsion and bending stresses; if  $h/2$  is the distance from the outer rim of the section to the central section line,

$$u^b(l) = \psi \frac{h}{2} \quad (12)$$

$$\text{and with } \epsilon_i^b = \frac{du^b}{dl} = \frac{h}{2} \frac{d\psi}{dl}; \quad \epsilon_\varphi^b = \frac{u^b}{r} = \psi \frac{h}{2r} \quad (13)$$

and using Hooke's law as applied to the displacement of the outer rim of section caused by bending, the result is:

$$\begin{aligned} \sigma_i^b &= \frac{E}{1-\nu^2} (\epsilon_i^b + \nu \epsilon_\varphi^b) \\ \sigma_\varphi^b &= \frac{E}{1-\nu^2} (\epsilon_\varphi^b + \nu \epsilon_i^b) \end{aligned} \quad (14)$$

If  $\epsilon^b$  is substituted by the corresponding terms, one obtains

$$\begin{aligned} \sigma_i^b &= \frac{Eh}{2(1-\nu^2)} \left( \frac{d\psi}{dl} + \nu \frac{\psi}{r} \right) \\ \sigma_\varphi^b &= \frac{Eh}{2(1-\nu^2)} \left( \nu \frac{d\psi}{dl} + \frac{\psi}{r} \right) \end{aligned} \quad (15)$$

$$\text{We obtain from the above equations } \psi = \frac{2r}{Eh} (\sigma_\varphi^b - \nu \sigma_i^b) \quad (16)$$

$$\text{and from the equations (10) } u = \frac{r}{E} (\sigma_\varphi - \nu \sigma_i) + r\alpha\vartheta \quad (17)$$

If these equations and their derivatives  $du/dr$  and  $d\psi/dl$  are incorporated in (10) and (15), taking into account also

$\beta = \tau/G - 2\frac{\tau}{E}(1+\nu)$ , we now obtain the wanted equations:

$$\nu \frac{d\sigma_i}{dl} - \frac{d\sigma_\varphi}{dl} + \frac{1+\nu}{r} (\sigma_i - \sigma_\varphi) \cos \delta + \frac{2}{h} \sin \delta (\sigma_\varphi^b - \nu \sigma_i^b) + \frac{2}{r} (1+\nu) \sin \delta \cdot \tau - E\alpha \frac{d\vartheta}{dl} = 0 \quad (18a)$$

$$\nu \frac{d}{dl} \left( \frac{1}{h} \sigma_i^b \right) - \frac{d}{dl} \left( \frac{1}{h} \sigma_\varphi^b \right) + \frac{1+\nu \cos \delta}{rh} \sigma_i^b - \frac{\cos \delta + \nu}{rh} \sigma_\varphi^b = 0 \quad (18b)$$

In his book "Calculation of Rotating Discs and Shells", K. Löffler offers the additional possibility of considering a linear distribution of temperatures in the direction of the normal to the medial area of the shell, which in this report will be mentioned only in passing and which offers no calculatory difficulty whatever.

### C) Inclusion of Blades, Rings and Bores

A consideration of radial blades or rings and bores, the latter being an exception, permits differential equations to be established in such a manner that these will change only with regard to their coefficients as opposed to the smooth shell, so that the new coefficients represent the sums total composed of the coefficients of the smooth shell and of certain additional members. The blading of the shells will now be considered first. In the following, the expression blades will frequently be replaced by the expression fins since by load application their function rather corresponds to that of a finned design.

#### a) The Altered Design of the Differential-Equations by Including the Existence of Fins

In view of the small azimuthal extent, the fins are assumed to be free from tangential stresses. If the longitudinal stress in the fin is expressed by  $\sigma_R$ , the following relation becomes valid due to the equal strain of fin and shell:

$$\sigma_R = \sigma_l - \nu \sigma_\varphi \quad (19)$$

If to the area of fin  $F_R$ , which may be assumed to be evenly distributed over the circumference, an equivalent thickness  $h' = z \cdot F_R / 2\pi r$  with  $z$  being the number of fins is added to the thickness of the shell, the equilibrium in the direction  $l$  is easily formulated.

$$d(\sigma_l h r d\varphi) - \sigma_\varphi h d l d\varphi \cos \delta + \tau h r d\varphi d\delta + d[(\sigma_l - \nu \sigma_\varphi) r d\varphi h'] + \tau h' r d\varphi d\delta + (h + h') d l r d\varphi \frac{\gamma}{g} \omega^2 r \cos \delta = 0 \quad (20)$$

For the sake of simplicity,  $\tau$  has in (20) also been assumed to be constant over the cross section of fin.

The equilibrium in the direction of shear and of the normal also results in

$$d[\tau r d\varphi (h + h')] - \sigma_\varphi h d\varphi d l \sin \delta - \sigma_l h r d\varphi d\delta - h' r d\varphi (\sigma_l - \nu \sigma_\varphi) d\delta + (h + h') d l r d\varphi \omega^2 r \sin \delta + p r d\varphi d l = 0 \quad (21)$$

The equilibrium of the moments around the direction of the tangents to a parallel circle must be established from the following components. If  $w$  is the moment of resistance referred to the circumference and relating to the finned cross section, the moment from the longitudinal stresses is

$$dM_l = d(\sigma_l^b r d\phi w) \quad (22)$$

The component in the direction of the tangent, taking into account the sign of the moment through tangential stress  $\sigma_\phi^b$  is obtained, as in the case of the smooth shell, as

$$M_\phi = -\sigma_\phi^b dl \frac{h^2}{6} d\phi \cos \delta \quad (23)$$

Figures 9 and 10 show the forces on a finned shell element as well as a representation of the further terms and designations employed. The shear stress in the shell furnishes a moment

$$M_{s_\tau} = \tau r d\phi h dl \frac{\sin d\delta}{d\delta} \quad (24)$$

and in the fin

$$M_{R_\tau} = \tau r d\phi h' dl' \frac{\sin d\delta}{d\delta} \quad (25)$$

$dl'$  being the mean length of fin which must be  $\lambda$  times as large as the length  $dl$  of the shell.

The geometry of Figure 10 yields

$$\begin{aligned} \varphi_2 &= \varphi_1 + \frac{1}{2} \left( \frac{h_{i-1} + h_i}{2} + s_{R_{i-1}} + s_{R_i} \right) \\ dl' &= \varphi_2 d\delta \quad ; \quad \varphi_1 = \frac{dl}{d\delta} \\ dl' &= dl + \frac{1}{2} \left( \frac{h_{i-1} + h_i}{2} + s_{R_{i-1}} + s_{R_i} \right) d\delta \\ \lambda = \frac{dl'}{dl} &= 1 + \frac{1}{2} \left( \frac{h_{i-1} + h_i}{2} + s_{R_{i-1}} + s_{R_i} \right) \frac{d\delta}{dl} \approx \frac{\Delta l'}{\Delta l} \end{aligned} \quad (26)$$

The radial components of the tangential stresses in the shell have around the centroid of the whole cross section a moment of

$$M_{\phi_s} = -\sigma_\phi h dl d\phi s \cos \delta \quad (27)$$

Similarly, a moment is produced by the longitudinal stress  $\sigma_l$  in the shell, which is of the following magnitude around the centroid

$$dM_{ls} = d(\sigma_l r d\phi h s) \quad (28)$$

The longitudinal stresses  $\sigma_R = (\sigma_l - \nu \sigma_\phi)$  produce a moment around the center of gravity

$$dM_{lR} = -d[(\sigma_l - \nu \sigma_\phi) r d\phi h s'] \quad (29)$$

As is shown in Figure 11,  $s$  indicates the distance of the centroid of the whole cross section from the central section line, and  $s'$  indicates the distance of the centroid of the fin cross section  $F_R$  from the whole centroid. If  $dM_{ls}$  and  $dM_{lR}$  are combined to

$$dM_{ls} + dM_{lR} = d\{\sigma_l [r d\phi (hs - h's')]\} - \nu d(\sigma_\phi r d\phi h s') \quad (30)$$

the term  $(hs - h's') = 0$  because of the equality of the statical moments.

The equilibrium of moments may be obtained from the following addition

$$dM_l + M_\phi + M_{s_\tau} + M_{R_\tau} + M_{R_s} + d(M_{ls} + M_{lR}) = 0 \quad (31)$$

For trapezoidal fins, the following terms are obtained to determine the moment of resistance of the whole cross section, using the signs of Figure 11:

$$s_R = \frac{h_R}{3} \frac{a+2b}{a+b}$$

$s_R$  being the centroid distance of the trapezoidal cross section from the larger basis  $b$ .

The distance of the whole cross section  $s$  from the central section line of the shell is

$$s = \frac{(a+b)h_R(s_R + \frac{h}{2})}{(a+b)h_R + \frac{4\pi R h}{2}}$$

The moment of resistance  $w$  is obtained by converting this term in such a manner that the moment of resistance of the smooth shell  $w_s = h^2/6$  referred to the circumference is given only another term

$$w = \frac{h^2}{6} + \frac{sh(6s-h)}{3(h+2s)} + \frac{\frac{h_a}{36} \frac{a^2+4ab+b^2}{a+b} + \frac{a+b}{2} h_a s'^2}{\frac{2\pi r}{2} (s + \frac{h}{2})} \quad (32)$$

The two differential equations yet to be found from the state of dilatation will be affected by the fins only insofar as in the term (15), and consequently also in the equations (18),  $h$  will be replaced by the length  $(h + 2s)$ , as the distance between the outer rim of the section and the central section line is no longer  $h/2$  but  $(h/2 + s)$ .

#### b) The Influence of Rings on the Differential-Equations

In view of the widely varying designs of radial compressor wheels or radial turbine wheels, cantilever-rings must frequently be taken into account which may be used as a form of packing, or the wheel body may be provided at the center bore with a hublike thickening which may be regarded as a ring zone being free from radial stresses. If such rings are considered as being free from radial stresses, this should apply only to narrow and thin designs of rings. Subject to the design of ring, however, an 'effective length' of a virtual equivalent ring can be determined which has a constant tangential stress in an axial direction. In his book "Calculation of Rotating Disks and Shells", K. Löffler included diagrams which have been evaluated by W. Burkhardt for rotating disks and which enable the above mentioned corrections to be made through the selection of an 'effective length'.

However, it would be beyond the scope of the present report to deal in greater detail with the problem of thin cantilever rings of marked projection, although the possible existence of cantilever rings should be duly taken into account.



For the sake of simplicity, the ring will in the following be considered as being completely free from radial stresses. Due to the tangential displacements being equal,

$$\sigma_{\varphi R} = \sigma_{\varphi} - \nu \sigma_i \quad (33)$$

As was already assumed in the case of the fins, the shearing stress will here again be considered to act as a mean and constant value even beyond the ring zone. Using the terms and forces plotted in Figure 12, the equilibrium of forces obtained at the shell element in the direction 1 leads to the following differential equation where forces being small in the higher powers have been disregarded:

$$d(\sigma_i h r d\varphi) - \sigma_{\varphi} h d l d\varphi \cos \delta + \tau h r d\varphi d\delta - (\sigma_{\varphi} - \nu \sigma_i) L d l d\varphi \cos \delta + \tau L r d\varphi d\delta + \frac{\delta}{g} r d\varphi (h+L) d l r \omega^2 \cos \delta = 0 \quad (34)$$

The equilibrium of forces in the direction of the shearing stresses will thus simply result in

$$d[r d\varphi (h+L) \tau] - [\sigma_{\varphi} h d l d\varphi + (\sigma_{\varphi} - \nu \sigma_i) L d l d\varphi] \sin \delta - \sigma_i h r d\varphi d\delta + \frac{\delta}{g} r d\varphi (h+L) d l r \omega^2 \sin \delta = 0 \quad (35)$$

The equilibrium of moments is again established around the direction of the tangents of the parallel circle through the central section line at  $(l + dl)$ . The bending stress  $\sigma_i^b$  produces in the shell the moment  $dM_i = d(\sigma_i^b r d\varphi \frac{h^2}{6})$  (36)

The same displacement is caused by the bending stresses on the virtual sectional areas between shell element and ring, under the term of

$$\sigma_{\varphi R}^b = \sigma_{\varphi}^b - \nu \sigma_i^b \quad (37)$$

$\sigma_{\varphi R}^b$  indicating the bending stress on the virtual sectional area acting on the ring in a tangential direction. As is shown in Figure 12, there is a relation

$$\frac{\sigma_{\varphi R}^b}{y} = \frac{\sigma_{\varphi R}^b}{\frac{h}{2}} \quad (38)$$

between the bending stress  $\sigma_{\varphi R}^b$  and the bending stress  $\sigma_{\varphi}^b$  at an arbitrary point of the ring and at a distance  $y$  from the center of shell.

The moment of bending stress  $\sigma_{\varphi}^b$  around the sectional line of the medial area of the shell with the lateral areas of the shell element bounded by  $d\varphi$  is

$$dM_R = \sigma_{\varphi}^b dy \cdot dl \cdot y \quad (39)$$

Adopting the equations (37) and (38), equation (39) leads to

$$dM_R = 2 \frac{y^2}{h} (\sigma_{\varphi}^b - \nu \sigma_t^b) dy dl \quad (40)$$

The linear connection  $\frac{\sigma_{\varphi}^b}{y} = \frac{\sigma_{\varphi_s}^b}{\frac{h}{2}}$  (41)

exists between the tangential bending stress on the outer rim of the shell  $\sigma_{\varphi}^b$  and the tangential bending stress  $\sigma_{\varphi_s}^b$  occurring at an arbitrary point with the distance  $y$  from the central section line.

The stress  $\sigma_{\varphi_s}^b$  thus produces at point  $y$  the moment

$$dM_s = \sigma_{\varphi_s}^b dy dl y = 2 \frac{y^2}{h} \sigma_{\varphi}^b dy dl \quad (42)$$

using term (41). The total moment from the tangential bending stresses is obtained by integrating  $dM_R$  and  $dM_s$

$$M_{\varphi}^* = \int dM_R + \int dM_s = 2 \frac{dl}{h} \int_{-\frac{h}{2}}^{+\frac{h}{2}} (\sigma_{\varphi}^b - \nu \sigma_t^b) y^2 dy + 2 \frac{dl}{h} \int_{-\frac{h}{2}}^{+\frac{h}{2}} \sigma_{\varphi}^b y^2 dy \quad (43)$$

Since  $\sigma_{\varphi}^b$  and  $\sigma_t^b$  act on the boundary areas of the shell, thus being constant values, the solution of (43) leads to

$$M_{\varphi}^* = \sigma_{\varphi}^b \left[ \left( 1 + 2 \frac{L}{h} \right)^3 + 1 \right] \frac{h^2}{12} dl - \nu \sigma_t^b \left[ \left( 1 + \frac{L}{h} \right)^3 - 1 \right] \frac{h^2}{12} dl \quad (44)$$

By introducing  $\xi = \frac{1}{2} \left[ \left( 1 + 2 \frac{L}{h} \right)^3 - 1 \right]$

the expression is abbreviated to

$$M_{\varphi}^* = \frac{h^2}{6} [(\xi + 1) \sigma_{\varphi}^b - \nu \xi \sigma_t^b] dl \quad (45)$$

Figure 13 illustrates the direction of the active moments and their resultant  $M_{\varphi}^* \cdot d\varphi$ . This Moment is produced by forces having their resultant in a radial direction. However, since the moment around the tangent of a parallel circle is wanted, it is only the component in the direction of  $\vec{l}$  that can be active;

it is therefore

$$M_{\varphi_1} = M_{\varphi_1}^* \cdot d\varphi \cdot \cos \delta \quad (46)$$

Another moment is caused by the radial component of the tensile stress  $\sigma_{\varphi R}$  existing in the ring. The force  $\sigma_{\varphi R} \cdot L \cdot dl \cdot d\varphi$  resulting from this stress is active at a distance  $1/2 (L + h)$  from the medial area of the blade. This moment acts positively or negatively, subject to the side of shell to which the ring is attached. On the convex side, i. e. the side **away from** the axis of rotation, the moment should be taken as positive. With the moment produced by the centrifugal force of the ring element,

$$M_{\varphi_2} = (\sigma_{\varphi R} L dl \frac{L+h}{2} d\varphi - \frac{\gamma}{g} \omega^2 r^2 d\varphi L dl \frac{L+h}{2}) \cos \delta \quad (47)$$

The cosine of angle  $\delta$  reappears here because only the components pointing in the direction  $\vec{l}$  of the forces  $\sigma_{\varphi R} \cdot L \cdot dl \cdot d\varphi$  and  $\gamma/g \cdot \omega^2 \cdot r^2 \cdot d\varphi \cdot L \cdot dl$  acting in a radial direction produce a moment in the prescribed direction. Equation (47) may be expressed more simply if the relation of displacement

$\sigma_{\varphi R} = \sigma_{\varphi} - \nu \sigma_t$  is used:

$$M_{\varphi_2} = (\sigma_{\varphi} - \nu \sigma_t - \frac{\gamma}{g} \omega^2 r^2) \frac{L+h}{2} L dl \cdot d\varphi \cos \delta \quad (48)$$

If the simplifying assumption of a constant shearing stress  $\tau$  existing over the shell and ring elements, the following moment through the shearing stress is obtained, analogously to the smooth shell:

$$M_{\tau} = \tau (h+L) dl r d\varphi \frac{\sin d\delta}{d\delta} \quad (49)$$

Taking into account the signs, the equilibrium of moments can be established with the elements  $dM_1$ ;  $M_{\varphi_1}$ ;  $\pm M_{\varphi_2}$  and  $M_{\tau}$ ,

$$dM_1 - M_{\varphi_1} \pm M_{\varphi_2} + M_{\tau} = 0 \quad (50)$$

or more minutely

$$d(\sigma_t^* r d\varphi \frac{h^2}{6}) - \frac{h^2}{6} [(\xi+1)\sigma_r^* - \nu \xi \sigma_t^*] dl d\varphi \cos \delta \pm (\sigma_{\varphi} - \nu \sigma_t - \frac{\gamma}{g} \omega^2 r^2) \times \\ \times L dl \frac{L+h}{2} d\varphi \cos \delta + \tau (h+L) dl r d\varphi \frac{\sin d\delta}{d\delta} = 0 \quad (51)$$

The three established equations designed to determine  $\sigma_l$ ,  $\sigma_\varphi$ ,  $\sigma_l^b$ ,  $\sigma_\varphi^b$  and  $\tau$  are supplemented by the differential equations established from the stress-strain relations for plain shells, the condition being that analogous to the finned shells the value  $h$  must be replaced by  $(h+1)$  in the differential equations (18).

c) The Influence of Additional Loads on the Differential-Equations

In establishing differential equations from the equilibria of forces or moments, outer additional loads may be taken into account without difficulty. These enlarge the differential equations by terms which will be dealt with in detail.

It should be observed that these additional loads are active at certain points of the shell, thus representing magnitudes which are taken from the geometry of the shell and which should no longer be introduced as variable but as constant values. If there is a radially acting additional load, which will be called  $P_z$ , the additionally occurring stress at the outer edge of a shell element with the radius  $r_1$  and a shell thickness  $h_1$  will be

$$\sigma_z = \frac{P_z}{2\pi r_1 h_1} \cos \delta_1 \quad (52)$$

The equilibrium of forces in the direction of a meridional section will thus be given another term, so that (1) now becomes

$$d(\sigma_l h r d\varphi) - \sigma_\varphi h dl d\varphi \cos \delta + \tau h r d\varphi d\delta + h dl r d\varphi \frac{\gamma}{g} r \omega^2 \cos \delta + \sigma_z r_1 d\varphi h_1 = 0 \quad (53)$$

The normal component of  $P_z$ , viz.  $P_z \cdot \sin \delta_1$ , occurs as an additional force in the equation of equilibrium (2) if

$$\tau_z = \frac{P_z \sin \delta_1}{2\pi r_1 h_1} \quad (54)$$

expresses the additional normal stress, and (2) is changed to become

$$d(\tau r d\varphi h) - \sigma_\varphi h dl d\varphi \sin \delta - \sigma_l h r d\varphi d\delta + h dl r d\varphi \frac{\gamma}{g} r \omega^2 \sin \delta + p r d\varphi dl + \tau_z r_1 h_1 d\varphi = 0 \quad (55)$$

If the additional load  $P_z$  comes to act at the distance  $k$  from the centroid of the section concerned, this will produce an additional moment of the magnitude

$$M_z = \sigma_z r_i d\varphi h_i k \quad (56)$$

This moment supplements the equation of equilibrium (5) in the form of

$$d(\sigma_i \frac{h^2}{6} r d\varphi) - \sigma_\varphi \frac{h^2}{6} dl d\varphi \cos \delta + \tau h dl r d\varphi \frac{\sin \delta}{d\delta} + \sigma_z r_i d\varphi h_i k = 0 \quad (57)$$

In view of the above, we can now write the differential equations in a general form so that they could be formulated for fins occurring in conjunction with rings and even additional loads. This, however, will be done later when the differential equations are compiled and the conversion of differential equations into equations of differences is illustrated by means of an example.

#### d) The Influence of Eccentric Circular Holes upon the Differential-Equations

When in the first approximation the zone of bore can be taken as free from tangential stresses, the stresses occurring at the beginning of the zone of bore can be immediately expressed by the stresses occurring at the end of the bore. This means that the relation between the stresses occurring immediately before and immediately behind the bore is not expressed in a differential equation but in a linear dependence. Stresses and geometric magnitudes at the beginning of the zone of bore will be marked with the index  $i-1$  and immediately behind the zone of bore with the index  $i$ . At first, the relation between the longitudinal stresses  $\sigma_{l_i}$  and  $\sigma_{l_{i-1}}$  will be dealt with.

$\sigma_{l_i}$  is determined from the equilibrium of forces on the spoke, i. e. the shell element between the bores.  $P_{sp}$  expresses the centrifugal force of the spokes,  $P_{schr}$  the centrifugal force

of the bolts or pins which may be inserted in the bores. The equilibrium of forces is now (see Figure 14)

$$P_i = P_{i-1} - (P_{sp} + P_{schr}) \cos \delta \quad (58)$$

If the forces are expressed by the stresses, this results in

$$\sigma_i 2\pi r_i h_i = (\sigma_{i-1} - \frac{P_{sp} + P_{schr}}{2\pi r_{i-1} h_{i-1}} \cos \delta) 2\pi r_{i-1} h_{i-1} \quad (59)$$

If we substitute

$$\frac{P_{sp} + P_{schr}}{2\pi r_{i-1} h_{i-1}} \cos \delta = \sigma_{sp} \quad (60)$$

we obtain

$$\sigma_i = \frac{r_{i-1} h_{i-1}}{r_i h_i} \sigma_{i-1} - \frac{r_{i-1} h_{i-1}}{r_i h_i} \sigma_{sp} \quad (61)$$

To enable a calculation to be made merely from the geometry of the shell and from the indication of the bolt weight  $G_{Schr}$ , a suitable description will now be found for  $\sigma_{sp}$ . This requires however that a few relations are established from the geometric conditions of the zone of bore.

The variable spoke section will be replaced by an equivalent rectangular section. The thickness of spoke is then

$$h_{sp} = \frac{1}{2} (h_i + h_{i-1})$$

The mean section of spoke  $F_{sp}$  can be determined only through determination of the volume of the spokes between the bores. According to Figure 14, the volume of the zone of bore (including the bores) is

$$V_R = \frac{r_i - r_{i-1}}{\cos \delta} h_{sp} \cdot \frac{r_i + r_{i-1}}{2} 2\pi$$

$$V_R = \frac{(r_i^2 - r_{i-1}^2) \cdot h_{sp} \cdot \pi}{\cos \delta}$$

The volume of n bores is

$$V_L = \frac{n}{4} \left( \frac{r_i - r_{i-1}}{\cos \delta} \right)^2 h_{sp} \cdot \pi$$

The volume of the spokes between the bores is

$$V = V_R - V_L$$

the mean section of spoke is

$$\begin{aligned} \bar{r}_{sp} &= \frac{V \cos \delta}{r_i - r_{i-1}} \\ \bar{r}_{sp} &= \left[ r_i + r_{i-1} - \frac{\pi}{4} \frac{r_i - r_{i-1}}{\cos \delta} \right] h_{sp} \cdot \pi \end{aligned}$$

Since  $\frac{r_i - r_{i-1}}{\cos \delta} = \Delta l$ , and using the abbreviation

$$t = \left[ r_i + r_{i-1} - \frac{\pi}{4} \Delta l \right], \quad F_{sp} = t h_{sp} \cdot \pi \quad (62)$$

The spoke force  $P_{sp}$  and the centrifugal force of the bolts  $P_{Schr}$  are expressed as follows

$$\begin{aligned} P_{sp} &= t h_{sp} \pi \frac{r_i - r_{i-1}}{\cos \delta} \cdot \frac{\gamma}{g} \omega^2 \frac{r_i + r_{i-1}}{2} \\ P_{Schr} &= G_{Schr} \frac{\omega^2}{g} \cdot \frac{r_i + r_{i-1}}{2} \end{aligned}$$

If  $P_{sp}$  and  $P_{Schr}$  are introduced in (60), the result is

$$\sigma_{sp} = \frac{\gamma \omega^2 (r_i + r_{i-1}) (t h_{sp} \Delta l + \frac{G_{Schr}}{\gamma \pi}) \cos \delta}{4 g r_{i-1} h_{i-1}} \quad (63)$$

We now want to formulate, by anticipation, a suitable coefficient for the establishment of a matrix yet to be dealt with,

$$c = \frac{\sigma_{sp} g}{\gamma \omega^2 r_{i-1}^2} = \left( 1 + \frac{r_i}{r_{i-1}} \right) \cos \delta \frac{t h_{sp} \Delta l + \frac{G_{Schr}}{\pi \gamma}}{4 r_{i-1}^2 h_{i-1}} \quad (64)$$

The tangential stresses may be brought into relation with the displacements. If a mean stress in the spoke is taken to be

$$\sigma_{spmi} = \frac{\sigma_{i-1} r_{i-1} h_{i-1} + \sigma_{ii} r_i h_i}{2 t h_{sp}} \quad (65)$$

this will produce in the spoke a displacement of

$$u_{sp} = \frac{l_i - l_{i-1}}{E} \sigma_{spmi} = \frac{\Delta l}{E} \sigma_{spmi} \quad (66)$$

The displacement at point i results in

$$u_i = u_{i-1} + u_{sp} \quad (67)$$

At points 1 and 1-1, the displacements are

$$\begin{aligned} u_{1-1} &= \frac{l_{1-1}}{E} (\sigma_{\psi_{1-1}} - \nu \sigma_{l_{1-1}}) - l_{1-1} \alpha_{1-1} \vartheta_{1-1} \\ u_1 &= \frac{l_1}{E} (\sigma_{\psi_1} - \nu \sigma_{l_1}) - l_1 \alpha_1 \vartheta_1 \end{aligned} \quad (68)$$

If (66) and (68) are introduced in (67), eliminating  $\sigma_{l_i}$  through the use of (61), the tangential stress  $\sigma_{\psi_i}$  will be obtained, which is dependent only on the stresses  $\sigma_{l_{i-1}}$  and  $\sigma_{\psi_{i-1}}$ , i. e. on values existing immediately before the zone of bore. The appropriately summarized result is

$$\begin{aligned} \sigma_{\psi_i} &= \frac{r_{i-1}}{r_i} \sigma_{\psi_{i-1}} + \frac{r_{i-1}}{r_i} \left[ \nu \left( \frac{h_{i-1}}{h_i} - 1 \right) + 2 \frac{\Delta l}{t} \cdot \frac{h_{i-1}}{h_{sp}} \right] - \\ &\quad - \frac{r_{i-1} h_{i-1}}{r_i h_i} \left( \nu + \frac{h_i \Delta l}{t h_{sp}} \right) \sigma_{sp} + \frac{\Delta l}{r_i} E \alpha (\vartheta_i - \vartheta_{i-1}) \end{aligned} \quad (69)$$

For the present purpose, the modulus of elasticity and also the linear coefficient of thermal expansion have been taken as constant over the length of spoke  $(l_1 - l_{1-1}) = \Delta l$ .

The relation between the moments is obtained if the equilibrium of moments around a tangent to a parallel circle is established at point 1. Moments are produced by  $\sigma_{l_i}^b$ ,  $\sigma_{l_{i-1}}^b$  and by the shear stress  $\tau_{i-1}$ . The equilibrium of moments is formulated with

$$\begin{aligned} M_{l_i} - M_{l_{i-1}} + M_{\tau} &= 0 \\ \sigma_{l_i}^b \frac{2\pi r_i h_i^2}{6} - \sigma_{l_{i-1}}^b \frac{2\pi r_{i-1} h_{i-1}^2}{6} + \tau_{i-1} \Delta l h_{i-1} 2\pi r_{i-1} &= 0 \\ \sigma_{l_i}^b &= \sigma_{l_{i-1}}^b \frac{h_{i-1}^2 r_{i-1}}{r_i h_i^2} - 6 \tau_{i-1} \frac{r_{i-1} h_{i-1}}{r_i h_i^2} \Delta l \end{aligned} \quad (70)$$

The relation between the tangential bending stresses immediately before and behind the zone of the bore is found by comparing the slopes at the beginning and end of the spoke (see Figure 15).

$$\psi_i = \psi_{i-1} + \Delta \psi \quad (71)$$

$\Delta \psi$  is the change of slope within the spoke. In order to arrive at the change of slope in the spoke, a mean moment of the magnitude



$$M_{sp} = \frac{M_i + M_{i-1}}{2}$$

$$M_{sp} = \frac{1}{2} (\sigma_{i,i}^b r_i 2\pi \frac{h_i^2}{6} + \sigma_{i,i-1}^b r_{i-1} 2\pi \frac{h_{i-1}^2}{6}) \quad (72)$$

according to Figure (15), is considered constant above the length of spoke  $\Delta l$ .

The equation of the deflection curve, where h in this case indicates the deflection, reads

$$\frac{d^2 h}{d l^2} = \pm \frac{M_{sp}(l)}{J E}$$

or

$$\frac{dh}{dl} = \pm \frac{1}{EJ} \int_0^{\Delta l} M_{sp}(l) dl + c_1 = \tan \Delta \psi \quad (73)$$

Since  $M_{sp}$  is independent of  $l$  the solution of (73) leads to

$$\frac{dh}{dl} = \pm \frac{1}{EJ} |M_{sp} l + c_1|_0^{\Delta l}$$

with  $l=0$ ,  $\frac{dh}{dl} = 0$ , and also  $c_1 = 0$ . As only small slopes occur, we may write

$$\Delta \psi \approx \tan \Delta \psi$$

The change of slope in the case of the spoke is

$$\Delta \psi = \frac{(\sigma_{i,i}^b r_i 2\pi \frac{h_i^2}{6} + \sigma_{i,i-1}^b r_{i-1} 2\pi \frac{h_{i-1}^2}{6}) \Delta l}{2 EJ} \quad (74)$$

The length of the axis of inertia is  $t\pi$ , and, consequently, the moment of inertia  $J = t\pi \frac{h_{sp}^3}{12}$ , which leads to

$$\Delta \psi = \frac{(\sigma_{i,i-1}^b h_{i-1}^2 r_{i-1} + \sigma_{i,i}^b h_i^2 r_i) 2 \Delta l}{E t h_{sp}^3} \quad (75)$$

The deflection of the disc at the points  $i-1$  or  $i$  is obtained from (see also equation 16))

$$\psi_{i-1} = \frac{2 r_{i-1}}{E h_{i-1}} (\sigma_{\varphi i-1}^b - \nu \sigma_{i,i-1}^b) \quad (76)$$

$$\psi_i = \frac{2 r_i}{E h_i} (\sigma_{\varphi i}^b - \nu \sigma_{i,i}^b)$$

The equations (75) and (76) are introduced in (71) to obtain

the new formulation for the deflection

$$\frac{2r_i}{Eh_i}(\sigma_{\psi_i}^b - \nu\sigma_{\psi_i}^b) = \frac{2r_{i-1}}{Eh_{i-1}}(\sigma_{\psi_{i-1}}^b - \nu\sigma_{\psi_{i-1}}^b) + \frac{2\Delta l}{Et h_{sp}^3} (r_{i-1} h_{i-1}^2 \sigma_{\psi_{i-1}}^b - r_i h_i^2 \sigma_{\psi_i}^b) \quad (77)$$

If, finally,  $\sigma_{\psi_i}^b$  is replaced by formulation (70) and (77) solved for  $\sigma_{\psi_i}^b$ , the result is an equation having on the right side only terms with the index i-1

$$\begin{aligned} \sigma_{\psi_i}^b = & \frac{r_{i-1} h_{i-1}}{r_i h_i} \sigma_{\psi_{i-1}}^b + \left[ 2 \frac{\Delta l h_{i-1}^2 h_i}{t h_{sp}^3} + \nu \left( \frac{h_{i-1}^2}{h_i^2} - \frac{h_i}{h_{i-1}} \right) \right] \frac{r_{i-1}}{r_i} \sigma_{\psi_{i-1}}^b - \\ & - 6 \frac{r_{i-1} h_{i-1}}{r_i h_i} \Delta l \left( \frac{\Delta r h_i^3}{t h_{sp}^3} + \nu \right) \tau_{i-1} \end{aligned} \quad (78)$$

The still lacking equation required to determine the five wanted stresses at the end of the zone of the bore is very easily obtained from the equilibrium of sectional forces which act normal to the spoke ends

$$\begin{aligned} \tau_{i-1} h_{i-1} r_{i-1} &= \tau_i h_i r_i \\ \tau_i &= \tau_{i-1} \frac{h_{i-1} r_{i-1}}{h_i r_i} \end{aligned} \quad (79)$$

Where bores are arranged in an annular way, the linear equations (61), (69), (70), (78) and (79) replace the corresponding differential equations as these were established, for instance, for the case of the smooth shell.

## 2. Application of the Matrix Calculus for the Determination of Stresses, the Differential-Equations having been Rewritten into Equations of Differences

### a) Compilation of the Differential-Equations

The differential equations will first be compiled in a general form, taking into account the presence of fins, rings and additional loads. As has been mentioned before, the coefficients of the general equations are sums of coefficients of the special differential equations from the smooth shell and of the additional coefficients resulting from the consideration of fins, rings and additional loads.

If divided by  $d\psi \cdot dl$ , five differential equations of the following form will result if

1.) the equations (1), (20), (34) and (53) are collated

$$\frac{d}{dl}[r(h+h')\sigma_i] + \nu L\sigma_i \cos \delta - \nu \frac{d}{dl} rh'\sigma_p - (h+L)\sigma_p \cos \delta + (h+h'+L)r\tau \frac{d\delta}{dl} + (h+h'+L)\frac{\gamma}{g}\omega^2 r^2 \cos \delta + \frac{1}{dl} r_i h_i \sigma_z = 0 \quad (80)$$

2.) Differential equation (18 a) alone, except that in the case of the fin in the coefficients appearing at  $\sigma_i^b$  the term  $h$  is replaced by the term  $(h + 2s)$ , and in the case of overlapping rings in the coefficients appearing at  $\sigma_p^b$  the term  $(h+L)$  must be introduced, which will lead to the generally valid form.

$$\nu \frac{d\sigma_i}{dl} + \frac{1+\nu}{r} \sigma_i \cos \delta - \frac{d\sigma_p}{dl} - \frac{1+\nu}{r} \sigma_p \cos \delta - 2 \frac{\nu}{h+2s} \sin \delta \sigma_i^b + \frac{2}{h+L} \sin \delta \cdot \sigma_p^b + \frac{2(1+\nu)}{r} \sin \delta \cdot \tau - E\alpha \frac{d\delta}{dl} = 0 \quad (81)$$

3.) Compilation of the differential equations (5), (31), (51) and (57)

$$\begin{aligned} & -3\nu(h+L)L\cos\delta\sigma_i + [3(h+L)L-6hs]\cos\delta\sigma_p + 6\nu\frac{d}{dl}(rh's'\sigma_p) + \\ & + 6\frac{d}{dl}(r\omega\sigma_i^b) + \nu h^2\zeta\cos\delta\sigma_i^b - h^2(1+\zeta)\cos\delta\sigma_p^b + 6\frac{\sin\delta}{d\delta}(h+\lambda h'+L)\tau - \\ & - 3(h+L)L\frac{\gamma}{g}\omega^2 r^2 \cos \delta - 6(k-s)\frac{r_i h_i}{dl}\sigma_z = 0 \end{aligned} \quad (82)$$

In (82), the factor (k-s) before the last term takes into account the distance of the active additional load from the axis of inertia of the finned cross section, while in (57) only the action of additional loads upon smooth shells was described.

4.) Generally valid differential equation according to (18 b)

$$\nu \frac{d}{dl} \left( \frac{1}{h+2s} \sigma_i^b \right) + \frac{1+\nu \cos \delta}{(h+2s)r} \sigma_i^b - \frac{d}{dl} \left( \frac{1}{h+L} \sigma_\varphi^b \right) - \frac{\nu + \cos \delta}{h+L} \sigma_\varphi^b = 0 \quad (83)$$

5.) Compilation of the differential equations (2), (21), (35) and (55) in the generally valid form

$$\begin{aligned} & \nu L \sin \delta \sigma_i - (h+h') r \sigma_i \frac{d\delta}{dl} - (h+L) \sin \delta \sigma_\varphi + \nu h' r \sigma_\varphi \frac{d\delta}{dl} + \\ & + \frac{d}{dl} [r(h+h'+L) \tau] + p r + (h+h'+L) \frac{d}{g} \omega^2 r^2 \sin \delta + \frac{r h_i}{dl} \tau_z = 0 \end{aligned} \quad (84)$$

It should be pointed out once more that the differential equations (80) through (84) have been formulated in such a manner as to assume the special, previously derived forms for smooth shells, fins, overlapping rings and additional loads if the geometric values which do not exist for a given case are assumed to equal zero.

#### b) Transformation of the Differential-Equations into Equations of Differences

The five linear differential equations describing the problem of the rotating shell may be converted into linear equations with small but finite differences if the functions contained in them are replaced by the arithmetic mean of their initial and terminal values of a sufficiently small section and if each differential is expressed by the difference of the two values of which it is formed. A function should be expressed as follows

$$F = \frac{F_i + F_{i-1}}{2} \quad (85)$$

If  $l$  for instance is to express the independent variable, a differential is replaced by a quotient of differences of the form

$$\frac{dF}{dl} = \frac{\Delta F}{\Delta l} = \frac{F_i - F_{i-1}}{l_i - l_{i-1}} \quad (86)$$

The differential equation (80) expressed in the form of differences will assume the following shape

$$\begin{aligned} & \frac{1}{\Delta l} [r_i(h_i + h'_i)\sigma_i - r_{i-1}(h_{i-1} + h'_{i-1})\sigma_{i-1}] + \frac{\nu}{2} (L_i \cos \delta_i \sigma_i + L_{i-1} \cos \delta_{i-1} \sigma_{i-1}) - \\ & - \nu \frac{1}{\Delta l} [r_i h_i \sigma_{\varphi_i} - r_{i-1} h_{i-1} \sigma_{\varphi_{i-1}}] - \frac{1}{2} [(h_i + L_i) \cos \delta_i \sigma_{\varphi_i} + (h_{i-1} + L_{i-1}) \cos \delta_{i-1} \sigma_{\varphi_{i-1}}] + \\ & + \frac{\delta_i - \delta_{i-1}}{2 \Delta l} [(h_i + h'_i + L_i) r_i \tau_i + (h_{i-1} + h'_{i-1} + L_{i-1}) r_{i-1} \tau_{i-1}] + \\ & + \frac{\gamma}{2g} \omega^2 [(h_i + h'_i + L_i + \frac{G \cdot r_s}{\pi \gamma \Delta l r_i^2}) \cos \delta_i r_i^2 + (h_{i-1} + h'_{i-1} + L_{i-1}) \cos \delta_{i-1} r_{i-1}^2] = 0 \quad (87) \end{aligned}$$

The last term of the equation (87) is obtained by substitution

$$\sigma_z = \frac{G r_s \omega}{2g \pi r_i h_i}$$

and by combining the corresponding coefficients in the term of the equation which is produced by the centrifugal force, i. e. attached with  $\omega^2 r^2 \frac{\gamma}{g}$ .  $G$  describes an additional load which has the distance of the center of mass  $r_s$  from the rotational axis. In a like manner as with equation (80), also equations (81) through (84) are converted into equations of differences, which however will not be demonstrated in detail here. If equation (87) is expressed with general coefficients and if the terms attached with  $i$  and  $i-1$  are put on different sides, the following equation is obtained:

$$\begin{aligned} & b_{00} \sigma_i + b_{01} \sigma_{\varphi_i} + b_{02} \sigma_i^b + b_{03} \sigma_{\varphi_i}^b + b_{04} \tau_i + b_{05} \frac{\gamma}{g} \omega^2 r_i^2 + b_{06} E_i \alpha_i \vartheta_i = \\ & = a_{00} \sigma_{i-1} + a_{01} \sigma_{\varphi_{i-1}} + a_{02} \sigma_{i-1}^b + a_{03} \sigma_{\varphi_{i-1}}^b + a_{04} \tau_{i-1} + a_{05} \frac{\gamma}{g} \omega^2 r_{i-1}^2 + a_{06} E_{i-1} \alpha_{i-1} \vartheta_{i-1} \quad (88) \end{aligned}$$

In equation (88), the coefficients

$$b_{02} = b_{03} = b_{06} = a_{02} = a_{03} = a_{06} = 0.$$

e) Application of the Matrix Calculus for Solving the Equations of Differences

The application of the method of differences with a view to determining the five wanted magnitudes is based on the technique of subdividing the shell into the smallest possible sections. If the terms of stress at the inner edge are known, those of the outer edge may be determined from the five given equations. While the calculation of the state of stress by means of transmission matrices appears to be rather tedious, the advantage offered by this method becomes obvious if it is considered that this method permits easy determination of store data in programmatic calculation where the time of calculation required by the high-speed computer is of minor importance. All geometric data can be immediately taken from the drawing, which together with the known boundary stresses, material constants etc. determine the number of storage data. If a stress vector of the form

$$S = \begin{bmatrix} \sigma_i \\ \sigma_p \\ \sigma_i' \\ \sigma_p' \\ \tau \\ \omega^2 r^2 \frac{\delta}{g} \\ E \cdot \alpha \cdot \delta \end{bmatrix} \quad (89)$$

is defined and all equations (81) through (84) are expressed in the form of differences, the set of equations will, in matrix form, assume the following form

$$BS_1 = AS_{1-1} \quad (90)$$

It should still be mentioned that another two equations have been added to the five differential equations, viz.:

$$\frac{\delta}{g} \omega^2 r_i^2 = \frac{\delta}{g} \omega^2 r_{i-1}^2 \left( \frac{r_i}{r_{i-1}} \right)^2 \quad (91)$$

and

$$E_i \alpha_i \vartheta_i = E_{i-1} \alpha_{i-1} \vartheta_{i-1} \frac{(E \alpha \vartheta)_i}{(E \alpha \vartheta)_{i-1}} \quad (91)$$

Equation (90) may be converted into

$$S_i = B^{-1} \cdot A S_{i-1} \quad (92)$$

thus establishing the relation between the outer and inner edge of the section. If there is the case of a shell with center bore, the stress terms  $\sigma_i$ ,  $\sigma_i^b$  and  $\tau$  at the inner and outer edge of the whole shell are usually known. An equation is therefore used which connects the stress vector  $S_o$  at the inner edge with the stress vector  $S_a$  at the outer edge.

At an arbitrary point  $i$  of the shell, there is a relation with

$$B_i^{-1} \cdot A_i = D_{i,i-1}$$

$$S_i = D_{i,i-1} \cdot D_{i-1,i-2} \cdot \cdot \cdot D_{2,1} \cdot D_{1,0} \cdot S_o = M_i \cdot S_o \quad (93)$$

Outer edge and inner edge of the shell, with  $n$  sections, are connected by

$$S_a = D_{n,n-1} \cdot D_{n-1,n-2} \cdot \cdot \cdot D_{i,i-1} \cdot \cdot \cdot D_{2,1} \cdot D_{1,0} \cdot S_o = M_a \cdot S_o \quad (94)$$

All matrices  $D_{i,i-1}$  may be easily determined, so that suitable defining equations may be selected from (94) to determine  $\sigma_\varphi$  and  $\sigma_\varphi^b$  at the inner edge. The inner edge vector  $S_o$  now being known, the vectors  $S_i$  can then be determined with the aid of (93) and (92). If there is no center bore, the defining equations

$$\sigma_{\varphi_o} - \sigma_{\varphi_o} = 0 \quad \text{and} \quad \sigma_{\varphi_o}^b - \sigma_{\varphi_o}^b = 0$$

will now offer themselves, since the stresses existing at the center of shell have no discrete direction and must therefore be equal. The latter courses of calculation clearly reveal the impossibility of calculating shells by means of table computers, as the establishment of coefficients for each section (the accuracy of the method being dependent upon the number of sections) would represent an unjustifiable

extent of calculation, so that matrix multiplication and matrix inversion of the form  $B^{-1} \cdot A$  are only practical by means of electronic computers. For the sake of completeness, term (90) will be represented in detail:

$$\begin{matrix}
 & B & & S_i & & A & & S_{i-1} \\
 \begin{bmatrix} b_{00} & b_{01} & 0 & 0 & b_{04} & b_{05} & 0 \\ b_{10} & b_{11} & b_{12} & b_{13} & b_{14} & 0 & b_{16} \\ b_{20} & b_{21} & b_{22} & b_{23} & b_{24} & b_{25} & 0 \\ 0 & 0 & b_{32} & b_{33} & 0 & 0 & 0 \\ b_{40} & b_{41} & 0 & 0 & b_{44} & b_{45} & 0 \\ 0 & 0 & 0 & 0 & 0 & 1 & 0 \\ 0 & 0 & 0 & 0 & 0 & 0 & 1 \end{bmatrix} & \cdot & \begin{bmatrix} \sigma_i \\ \sigma_\varphi \\ \sigma_i^b \\ \sigma_\varphi^b \\ \tau \\ \omega^2 r^2 / g \\ E \alpha \vartheta \end{bmatrix} & = & \begin{bmatrix} a_{00} & a_{01} & 0 & 0 & a_{04} & a_{05} & 0 \\ a_{10} & a_{11} & a_{12} & a_{13} & a_{14} & a_{15} & a_{16} \\ a_{20} & a_{21} & a_{22} & a_{23} & a_{24} & a_{25} & 0 \\ 0 & 0 & a_{32} & a_{33} & a_{34} & 0 & 0 \\ a_{40} & a_{41} & 0 & 0 & a_{44} & a_{45} & 0 \\ 0 & 0 & 0 & 0 & 0 & a_{55} & 0 \\ 0 & 0 & 0 & 0 & 0 & 0 & a_{66} \end{bmatrix} & \cdot & \begin{bmatrix} \sigma_{i-1} \\ \sigma_\varphi \\ \sigma_i^b \\ \sigma_\varphi^b \\ \tau \\ \omega^2 r^2 / g \\ E \alpha \vartheta \end{bmatrix} \\
 & & & i & & & & i-1
 \end{matrix} \quad (95)$$

In the case of a zone of bore which is free from tangential stress, (95) is replaced by a corresponding matrix equation which is formed of equations (61), (69), (70), (78) and (79). Here matrix B has covered only the main diagonal with the coefficients 1. In matrix A the coefficients are arranged in the same manner as for instance in (95). A representation of the various coefficients may be dispensed with; as is shown in example (87), these may however be easily determined.



## II. Description and Graphic Representation of Results from the Theoretical Stress Determination

### 1. Results with Impeller-Wheels whose Geometrical Shapes were Chosen Systematically

The diversified designs of impeller wheels cannot be easily classified systematically. A possibility of determining the influence of different wheel designs upon their strength would be to compile a catalog of the course of stresses in manufactured wheels, arranging them by certain design characteristics etc. The investigations conducted by the "Institut für Turbomaschinen" at the Aachen Technical University on strength problems of impeller wheels are aimed at introducing a certain systemization in the wheel profile whereby the dependence of the stress terms on a single design parameter is investigated. Where the parameter passes different values, one possible wheel design will be maintained. In the initial equations for the calculations concerning rotating shells, the geometry of the shell yields definable magnitudes which may be individually varied, while all the others are kept constant, in order to determine in this way the influence upon the strength. The most interesting variation is to be found here in the different slopes of the shell to a plane located vertical to the axis of rotation, which so far had been understood to be the angle of slope of a meridional section of the medial area of the shell.

However, in general the slope  $\delta$  is not constant over the extent  $l$  of the meridional section. To describe the meridional curve, a function of the form

$$y = k [1 - \cos(1,333\pi\hat{r}) + \hat{r}^2]$$

was selected, the y-axis being the rotational axis. The abscissa  $\hat{r}$  represents a relative length

$$\hat{r} = \frac{x}{L - \Delta l}$$

In this term,  $x$  is the independent variable and  $L = \sum \Delta l$  ; the length of line of the meridional curve which is to be kept constant. Figure 16 shows the selected function with different parameters  $k$ . Also plotted were curves of equal length of line with a constant distance  $\Delta l$ . The selected function has the property of a descent to zero ( $\delta_o = 0$ ) at  $\hat{r} = 0$  for all values of  $k$ , while over the extent 1 for  $\hat{r} > 0$  the ascent rises with  $k$  at points of constant length of line. In Figure 17, the wheel design for  $k = 0,0625$  has been plotted as a full line, and for  $k = 0,375$  as a dashed line, both wheel designs having the same thickness  $h$  of shell and equal dimensions for the blades at the points  $l = \text{constant}$ , so that in the store data of the programmatic calculation merely the slope of shell  $\delta_{i,i-1}$  at the sections  $\Delta l_i$  was introduced differently for each varying  $k$ .

The following Figures 18, 19, 20 and 21 show the five calculated specified stresses of the systematically varied contours. The stiffening of the profile by means of blading has a noticeable effect along the longitudinal bending stress  $\sigma_l^b$  and, although in a less marked degree, upon the tangential bending stresses  $\sigma_\varphi^b$ . The longitudinal bending stresses show a considerable drop in the places where the blades begin.

2. Theoretical Stress Distribution in the Test Models. Especially with Respect to the Influences of the Blade Number, the Poisson Ratio, and Temperature Fields

Figure 22 shows the stresses in a model designed for initial experimental investigations, wherein the rear of the impeller wheel was kept plane (hatched distribution of stresses), and, on the other hand, has the contour illustrated in the drawing (strong, unbroken line for the stress distribution). As another comparison, Figure 22 shows the weaker unbroken line of the tangential and radial stresses in the wheel body which was also machined on the rear, if- as was said already in the beginning of the report- the impeller wheel is assumed to be a symmetric disc and if the blades are taken into account with regard to the increase of thickness of the shell profile proper or to their specific gravity. The increase of thickness  $h'$  is represented by a hatched line in Figure 22. The strongly projecting shell portion near the hub of the impeller wheel front side was taken in the calculation as a ring zone being free from radial stresses. The design of the wheel body of the built model was furthermore intended to enable the influence of different blade numbers to be studied, which is shown in Figure 23.

The influence exercised by Poisson's ratio is of minor importance. The calculation of the dimensionless stresses  $\sigma : (\rho \cdot r^2 \cdot \omega^2)$  was carried out with different Poisson's ratios  $\nu = 0,3$  and  $\nu = 0,36$ . The maximum deviation was determined as 5,6 percent for the stresses  $\sigma_r^b$ . Figure 24 shows the change in the stresses for three different temperature patterns illustrated in Figure 25, the entry of shearing stresses having however been dispensed with for the sake of diagrammatic clarity.

### 3. Superposition of Stresses

It should be pointed out once more that the calculated bending stresses apply to the rear end of the impeller wheels. On the front side of the wheels - if the shell is unbladed -, they possess the same absolute value of reversed sign. If there are blades and if  $s$  represents the distance of the central line from the medial area of the wheel, the longitudinal bending stresses  $\sigma_i^{b'}$  on the front edge of the blade are calculated on the following equation (see Figure 26):

$$\sigma_i^{b'} = - \frac{h_R + \frac{h}{2} - s}{\frac{h}{2} + s} \sigma_i^b \quad (96)$$

The bending stresses are additively superposed on the normal stresses, so that subject to the sign of the bending stresses on the rear of the wheel body considerable boundary stresses may occur in the front edges of blade, as established by the theoretical calculation. In Fig. 26, the superposition of  $\sigma_i^b$  and  $\sigma_i$  is illustrated once for negative bending stresses occurring on the rear of the shell (shown by the hatched line) and, on the other hand, for positive bending stresses (shown by the unbroken line).

### III. Measurement of Stresses with the Rotating Model

#### 1. Description of Model Design and Material

The measuring of stresses on the rotating model must be largely confined to measuring the stresses occurring on the surface of the wheel body as it is only here that a state of plane stresses exists. The wheel design selected for the first measurement is illustrated in its main dimensions in Figure 27. The shell body proper was made of plexiglas in the model which was built first. In radial slots milled out of the smooth shell, four blades of uniform thickness  $a = 1$  cm and made of VP 1527 material were cemented. Later on another model of like dimensions was built whose wheel body was made of VP 1527. Two pairs of opposite blades, which were cemented just on the surface of the shell front side, were made of VP 1527 and of Araldit-B, respectively.

The low number of four blades was selected in order to enable these to be stroboscopically tested vertical to the axis of rotation. As formerly only rotary speeds of up to  $n = 6000$  RPM could be reached, one pair of blades in the second model was made of Araldit-B which has a superior photoelastic action. The excessive blade thickness  $a$ , which does not meet actual conditions in impeller wheels, is largely compensated by the low number of four blades, so that with equal blade volume but normal blade thicknesses a roughly equivalent blade number  $z = 15 \div 18$  would result.

## 2. Scheme of the Test Arrangement

The complete testing equipment is illustrated in Figure 29. While Figure 30 sketches the path of light for the stroboscopic penetration of blade by means of flash lamp F, mirrors  $S_1$  and  $S_2$ , polarizer P, model M, analyzer A and camera K, Figure 31 illustrates the measuring scheme for measurements with strain gages where  $R_1$  designates the active strain gage,  $R_2$  the compensator, A the rotational transmitter, B the carrier frequency measuring bridge and C the switch for different strain gages mounted on the model. The strain gages were first mounted only in symmetrical places of the impeller wheel as the direction of principal stresses is known only in these places. The strain measurements were carried out in corresponding places both in a radial and tangential direction. The principal stresses result with the known strains  $\epsilon_1$  and  $\epsilon_2$  in

$$\begin{aligned}\sigma_1 &= \frac{E}{1-\nu^2} (\epsilon_1 + \nu\epsilon_2) \\ \sigma_2 &= \frac{E}{1-\nu^2} (\epsilon_2 + \nu\epsilon_1)\end{aligned}\tag{97}$$

### 3. Test Procedure and Preliminary Results

Measurement of the stresses and strains were conducted in such a manner that the photoelastic behavior of the blades and the strains occurring in certain places of the wheel body could be simultaneously observed with the aid of the strain gages. Figure 32 shows the fringe picture of a transilluminated blade made of the photoelastically active Araldit-B material at a rotational speed of  $n = 6000$  RPM. An exact quantitative analysis of stresses in the blades is impractical due to the low fringe order at the speeds so far attained. With the aid of a suitable carrier frequency measuring bridge, the strains may be read off as a function of the speed. In view of the very high linear heat extension of the synthetic resins that were used in constructing the models, the temperature compensation was found to be fairly difficult as temperature differences of very few degrees occurring between the places where the strain gages were mounted and in the places where the compensation gages are located will be sufficient to produce impermissible deviations in the measurements. The compensation gages were cemented on in places where there are no stresses, although they were exposed during the test to the temperature variations of the ventilated air. On the rotating model, the front edge of blade at the outer radius  $r_a$  offers itself as a stress-free portion of the impeller wheel. Further tests aimed at compensation were attempted in such a manner that unloaded plastic rods to carry the compensation gages were statically attached to the periphery of the rotating wheel, and were thus also exposed to the ventilated air flow from the impeller wheel. Figure 33 shows the measured stresses in the symmetric section between two blades on the front side of shell. In view of the considerably local variation of stresses anticipated, strain gages of metal foil with as small a measuring surface as possible were employed.

#### 4. Remarks on the Continuation of the Test Program

In continuation of these tests, the models of the coming experiments will be coated with brittle lacquer in order to localize the severest stresses in these places where the grids of cracks reveal the greatest density of lines. In addition to that, the crack lines extending at right angles to the direction of the major principal stress are expected to furnish information on the direction of the principal stresses, so that the strain gages may be applied to any desired place of the model in a corresponding direction. Strain gages which are arranged in a rosette fashion and permit the stress conditions to be completely covered without any knowledge of the direction of principal stresses being required, possess too large a measuring surface where the stresses may be subject to severe changes.

For necessary higher speeds, a direct current shunt motor of greater power will be installed which will be controlled in its speeds by Ward-Leonard operation. The required speeds of up to  $n = 25,000$  RPM will be obtained by a gear. Speed measurement will be made with utmost accuracy through direct digital registration.



## B I B L I O G R A P H Y

- /1/ Adams, E. W.: Festigkeitsrechnung der Mittelscheiben rotierender axialer Turboküfer mit beliebigem drehsymmetrischem Scheibenprofil unter Berücksichtigung der Spannungserhöhung durch die Flügel. Diss. Darmstadt (1956)
- /2/ Biezeno, C. B., a. R. Grammel: Technische Dynamik. Bd. I a. II, 2. Auflage 1953, Springer-Verlag, Berlin/Göttingen/Heidelberg.
- /3/ Bosch, M. Ten: Berechnung der Maschinenelemente. 3. Auflage 1951, Springer-Verlag, Berlin/Göttingen/Heidelberg.
- /4/ Dietrich, O., a. E. Lehr: Das Dehnungslinienverfahren. Z. VDI 76 (1932), S. 973/82.
- /5/ Donath, M.: Die Berechnung rotierender Scheiben und Ringe nach einem neuen Verfahren. Berlin 1929.
- /6/ Durelli, A. J., a. S. Okubo: Crack density studies in stress coat. Proc. Soc. exper. Stress Anal. 11 (1953) Nr. 1, S. 18/96.
- /7/ Eck-Kearton: Turbogebälse und Kompressoren. Springer-Verlag 1929, S. 111.
- /8/ Fink, K., a. Chr. Rohrbach: Handbuch der Spannungs-Dehnungsmessung. VDI-Verlag Düsseldorf 1958.
- /9/ Fink, K.: Der Dehnungsmeßstreifen. Z. VDI 92 (1950), S. 89/94 a. 176.
- /10/ Flüge, W.: Statik und Dynamik der Schalen. Springer-Verlag 1934.
- /11/ Flüge, W.: Stresses in Shells. Springer-Verlag 1960, Berlin/Göttingen/Heidelberg.

- /12/ Föppel, L., a. E. Mönch: Praktische Spannungsoptik. Springer-Verlag 1959, Berlin/Göttingen/Heidelberg.
- /13/ Frocht, M. M.: Photoelasticity. Vol. I, II, Fourth Printing, 1957, New York, John Wiley & Sons, Inc.
- /14/ Geckeler, J. W.: Theorie der Elastizität flacher, rotationssymmetrischer Schalen. Ing.-Arch. Bd. 1 (1930), S. 255.
- /15/ Grammel, R.: Neue Lösungen des Problems der rotierenden Scheibe. Ing.-Arch. Bd. 7 (1936), S. 137.
- /16/ Hodge, P. G., a. J. Papa: Rotating disks with no plane of symmetry. J. Franklin Inst. (June 1957).
- /17/ Honegger, E.: Festigkeitsrechnung von rotierenden konischen Scheiben. Z. angew. Math. Mech., Bd. 7 (1927), S. 120.
- /18/ Jaburek, F.: Die Festigkeit von radialbeschauelten Laufrädern. Österr. Ing.-Arch. VII (1953), Nr. 3.
- /19/ Karas, K.: Zur Berechnung rotierender Scheiben vorgegebenen Profils. Österr. Ing.-Arch. IX (1955), S. 157.
- /20/ Kasperek: Wärmespannungen in Dampfturbinenrädern. Z. ges. Turbinenw. Bd. XIV (1917) Nr. 4, S. 32.
- /21/ Keller, C.: Die Berechnung rotierender Scheiben mit Hilfe von konischen Ringen. Escher. Wyss Nachr. (1932).
- /22/ Knauer, G.: Festigkeit achsensymmetrischer Schalen unter drehsymmetrischer Belastung berechnet mittels schrittweiser Integration. Diss. Aachen (1957).

- /23/ Kuske, A.: Einführung in die Spannungsoptik. Wiss. Verlagsgesellschaft m.b.H. Stuttgart (1959).
- /24/ Langhaar, H. C.: Dimensional Analysis and Theory of Models. John Wiley & Sons, Inc. New York, 1951.
- /25/ Löffler, K.: Die Berechnung von rotierenden Scheiben und Schalen. Springer-Verlag 1961, Berlin/Göttingen/Heidelberg.
- /26/ Malkin, J.: Festigkeitsberechnung rotierender Scheiben. Berlin 1935.
- /27/ Manson, S.: Determination of elastic stresses in gas turbine disks. NACA-Report Nr. 871 and Naca TN 1279.
- /28/ Münch, E.: Die Ähnlichkeits- und Modellgesetze bei spannungsoptischen Untersuchungen. Z. angew. Phys., Bd. 1 (1949).
- /29/ Müller, K. J.: Die Festigkeit rein radial beschauelter Kreiselverdichter-Laufräder. Österr. Ing.-Arch. Bd. II (1948), S. 138.
- /30/ Ostertag, P.: Kolben- und Turbokompressoren. Springer-Verlag Berlin 1923, S. 229.
- /31/ Parkus, H.: Wärmespannungen in Rotationsschalen bei drehsymmetrischer Temperaturverteilung. S.-B. Österr. Akad. Wiss., Abt. II, 2, 160, I (1951).
- /32/ Pflüger, A.: Einführung in die Schalenstatik. Wiss. Verlagsanstalt K. G. Hannover (1948).
- /33/ Salzmann, F., a. W. Kissel: Kurvenscharen zur Berechnung der Spannungen in rotierenden und ungleichmäßig erwärmten Scheiben nach dem Verfahren von Keller. Escher Wyss-Dampfturbinen (1950/51), S. 69.

- /34/ Stodola, A.: Dampf- und Gasturbinen. Springer-Verlag Berlin 1924.
- /35/ Timoschenko, S.: Theory of plates and shells. New York/London 1940.
- /36/ Unger, H.: Matrizenverfahren bei linearen Differentialgleichungsproblemen. Internat. Kolloquium über Probleme der Rechentechnik. Dresden (1955).
- /37/ Wlassow, W. S.: Allgemeine Schalentheorie und ihre Anwendung in der Technik. Akademie-Verlag Berlin (1958).
- /38/ Wolf, H.: Spannungsoptik. Springer-Verlag 1961, Berlin/Göttingen/Heidelberg.
- /39/ Zurewühl, R.: Matrizen. Springer-Verlag 1958, 2. Aufl., Berlin/Göttingen/Heidelberg.

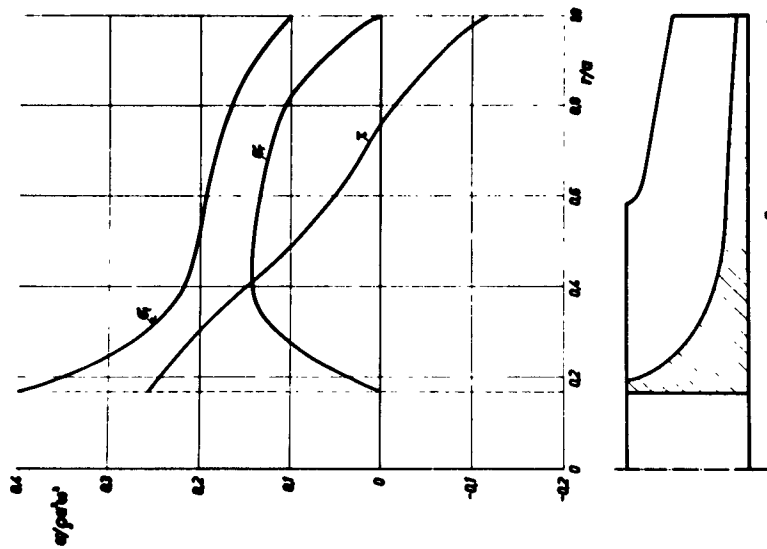


Fig. 1

Stresses of an impeller wheel calculated by the method of K. J. Müller

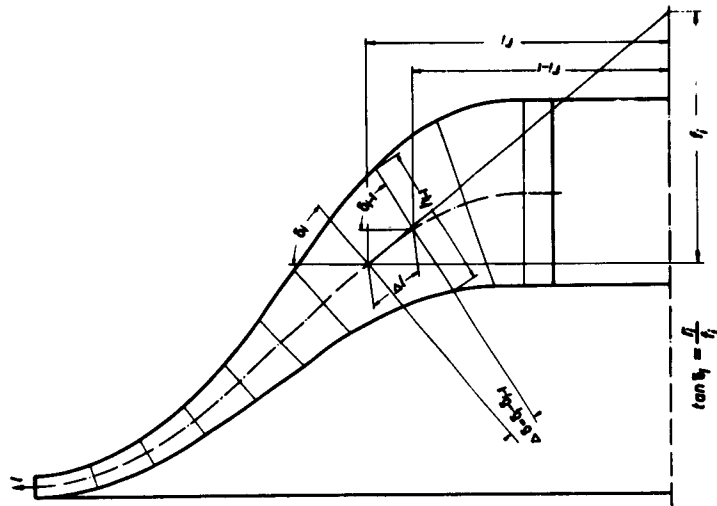


Fig. 2

Specimen of a shell disassembled into sections, with corresponding designations used in the calculations.

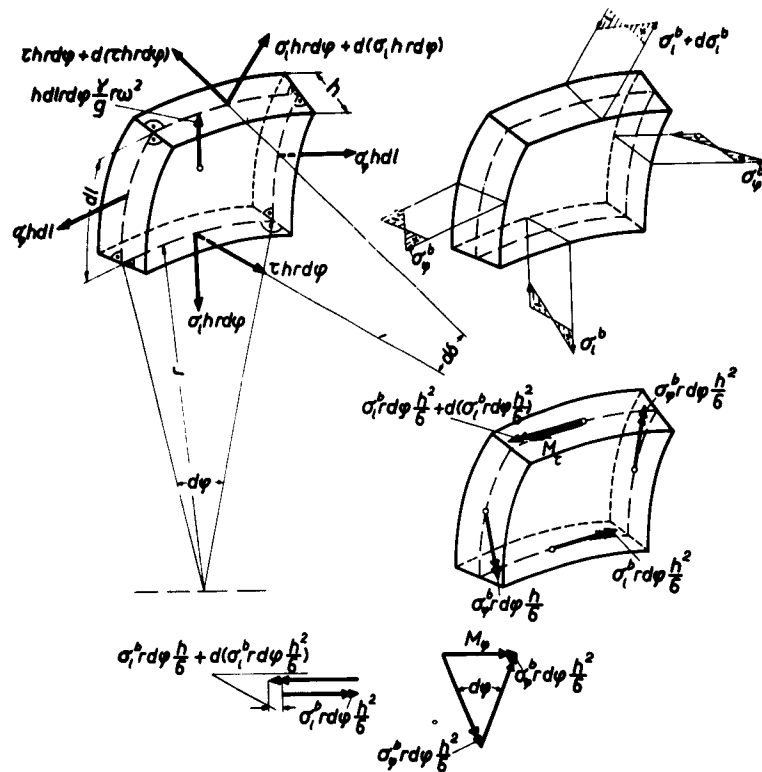


Fig. 3  
Forces and moments acting on the shell element. The sectional areas are formed on the one hand by surface lines and on the other hand by parallel circles, and are positioned perpendicular to the medial area of shell.

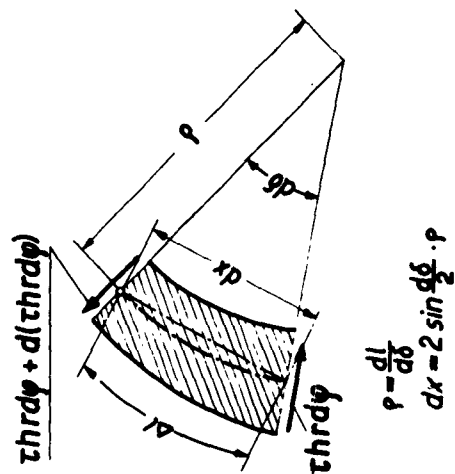


Fig. 4  
Comments on the formulation of the moment  
through the shear stress

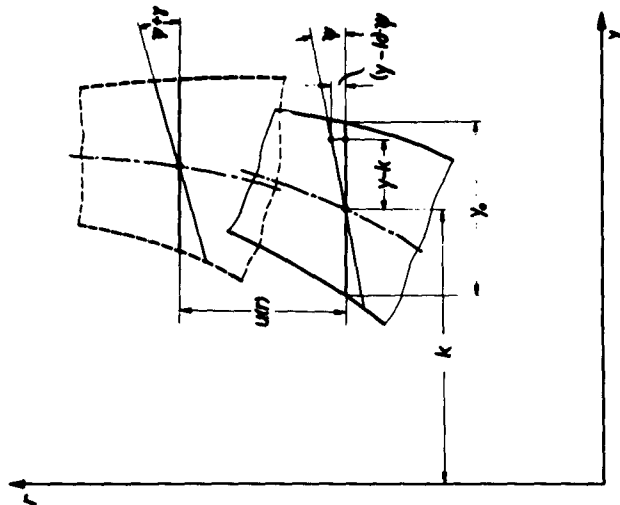


Fig. 5  
Displacements of an arbitrary point on a cylindric  
section of the shell

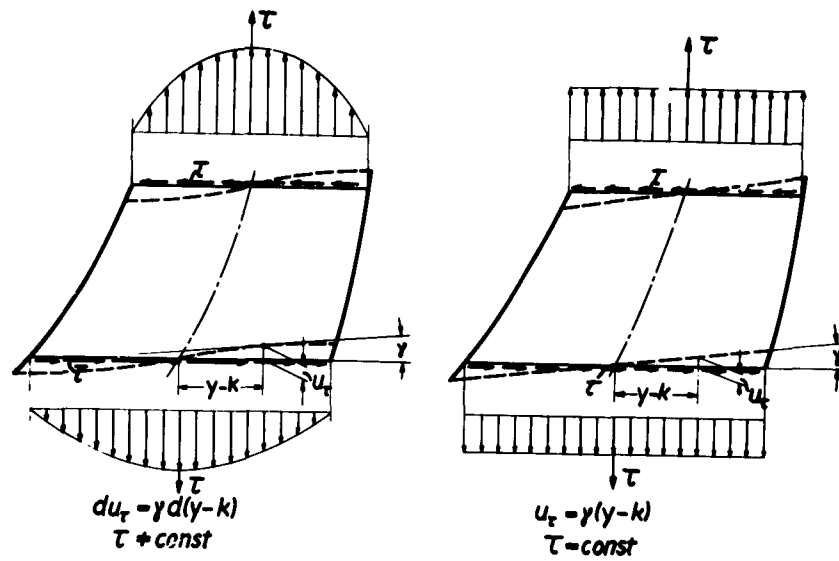


Fig. 6  
Shear deformation on the shell element for  $\tau = \text{const}$  and  $\tau = \text{const}$

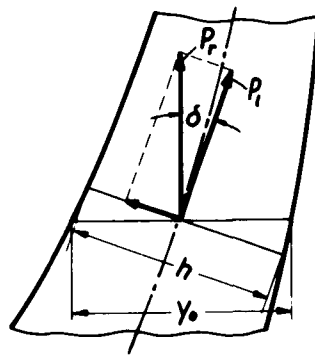


Fig. 7  
Relation between radial stress and longitudinal stress



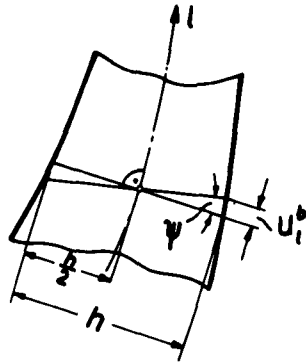


Fig. 8  
Comments on the relation between  
slope and bending stress

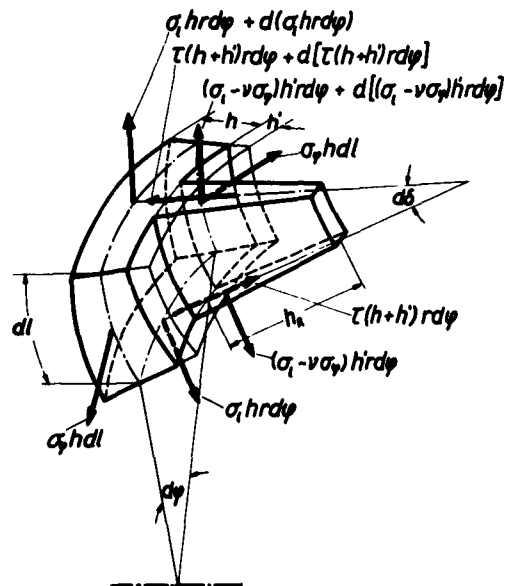


Fig. 9  
Designations and forces on the finned shell element

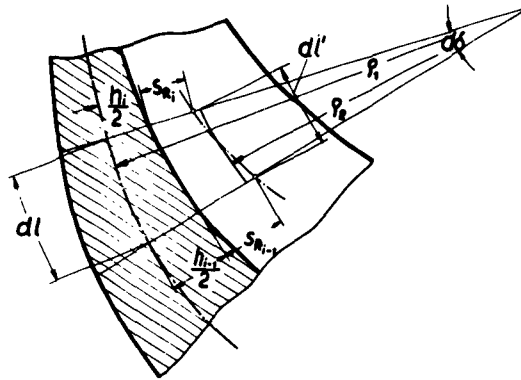


Fig. 10  
Comments on the geometric relations for the mean  
length of fin  $l'$

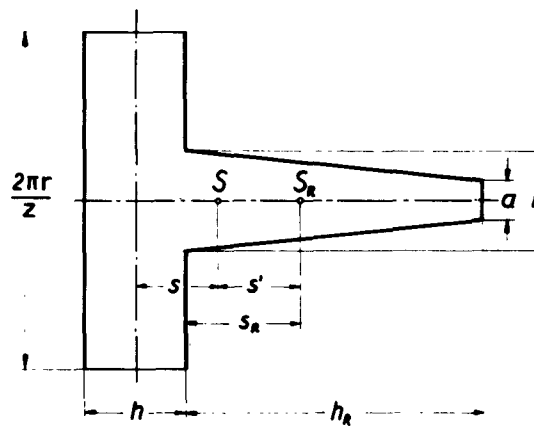


Fig. 11  
Illustration of the geometric dimensions and  
terms of a shell with fin

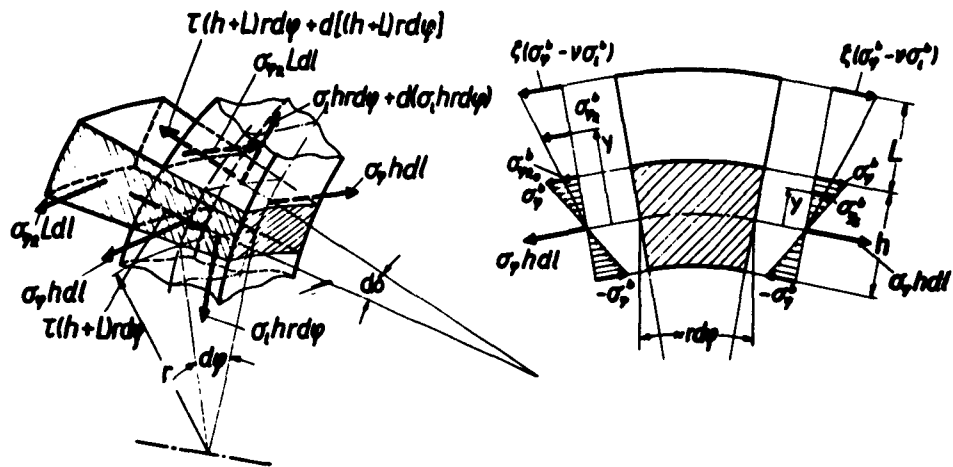


Fig. 12  
Equilibrium of forces in shell and ring as well as relation between bending stresses in the shell and ring being free of longitudinal stress

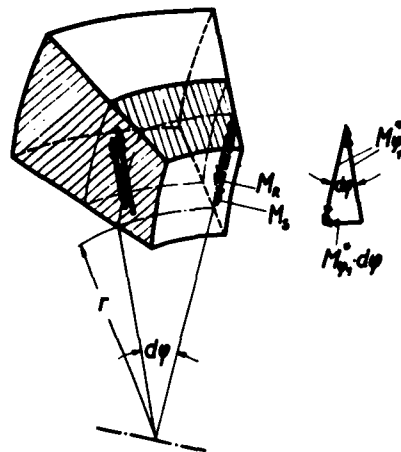


Fig. 13  
Moments on the shell element with ring zone

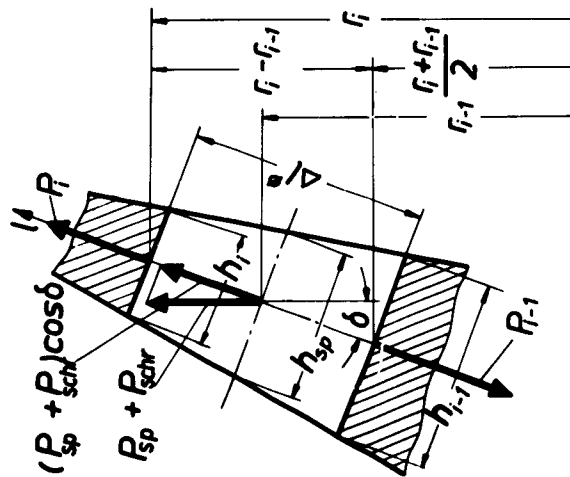


Fig. 14  
Equilibrium of forces in the bore zone of shell

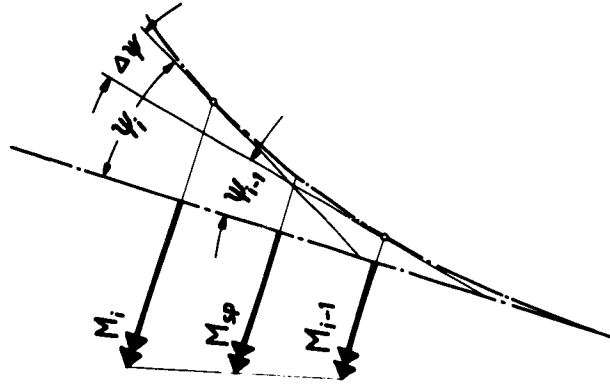


Fig. 15  
Slopes and moments on a 'spoke'

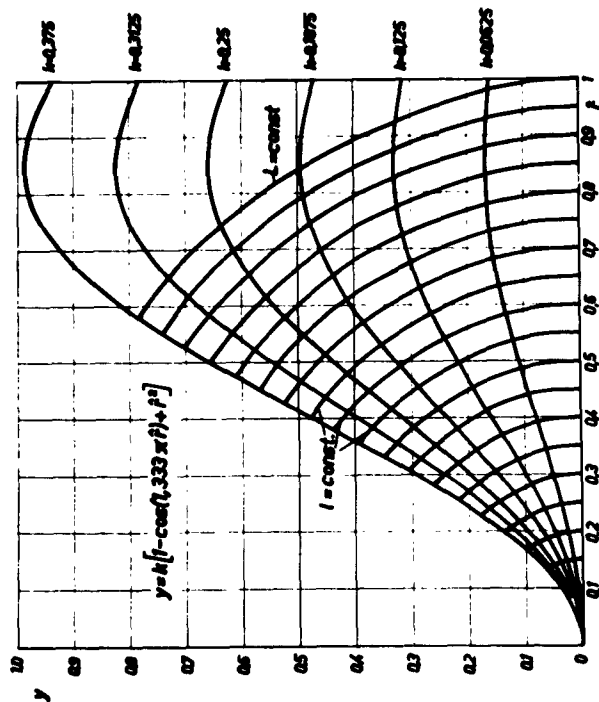


Fig. 16  
Graphic representation of the function of the meridional section of the medial shell area with different parameters  $k$  to the variation of the shell contour

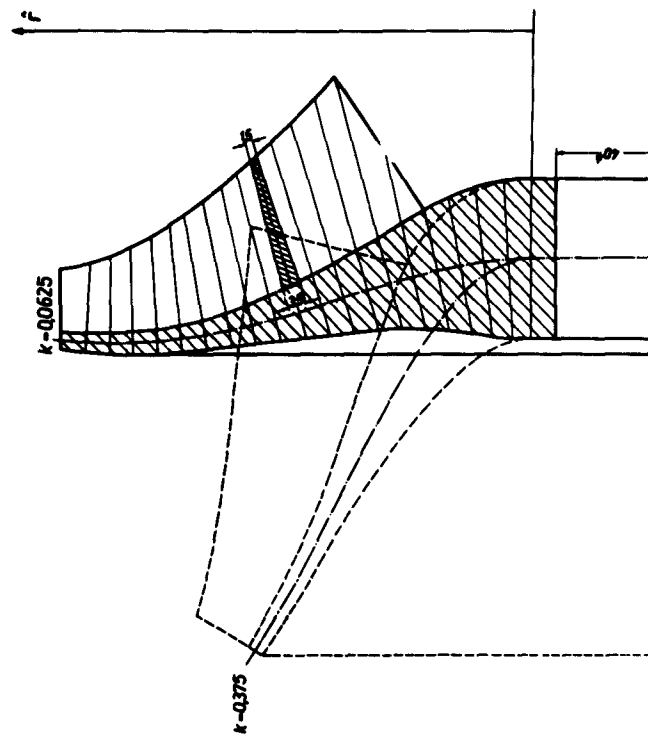


Fig. 17  
Representation of possible wheel design whose contours were varied systematically

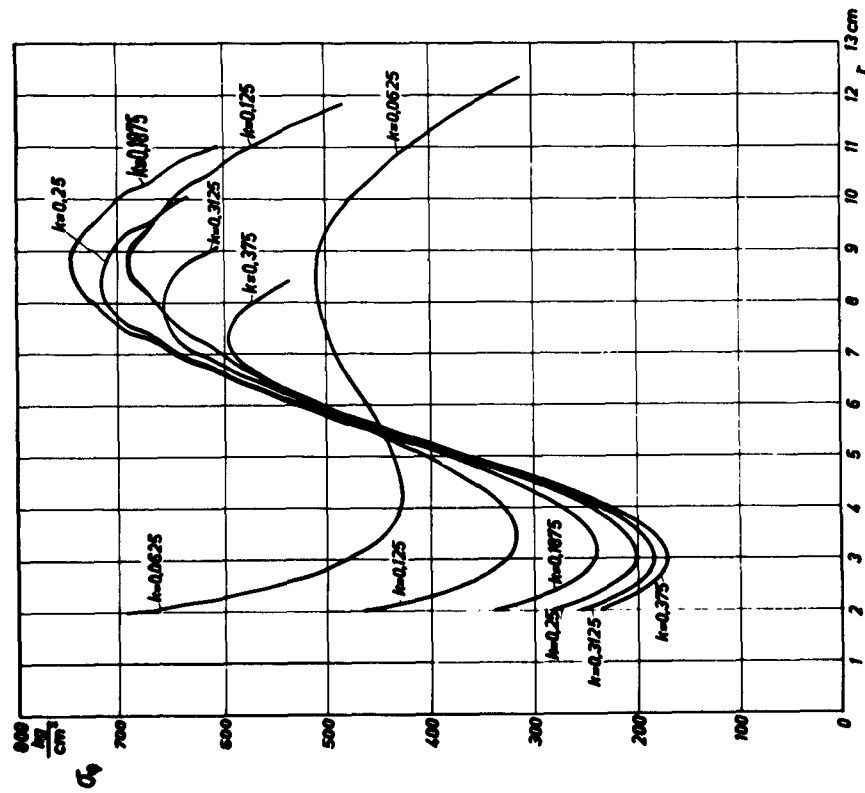


Fig. 18  
Representation of the tangential stress  $\sigma_\theta$  with varied parameters  $k$  of the contour-determining function of meridional contour

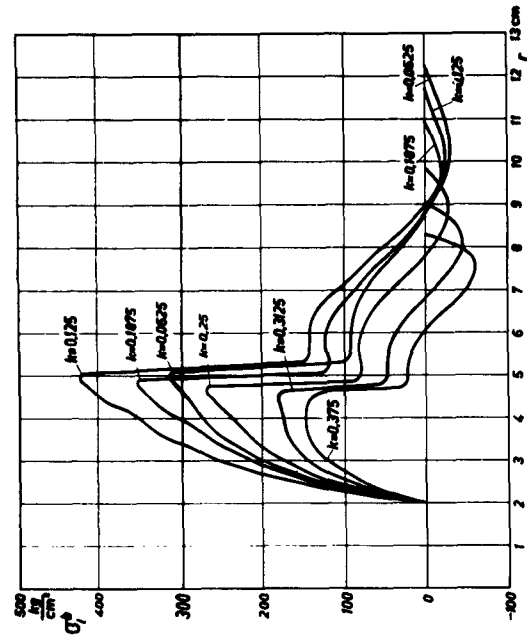


Fig. 19  
Analogous to Fig. 18, representation of the longitudinal bending stress  $\sigma_x$

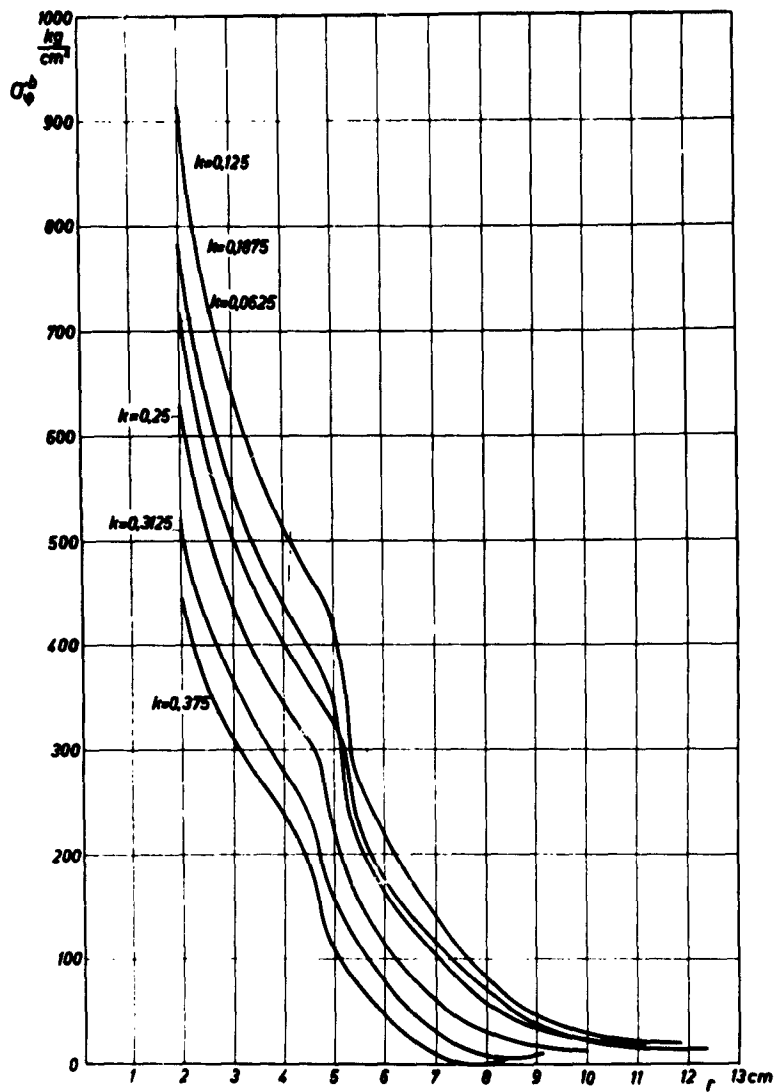


Fig. 20  
Analogous to Fig. 18, representation of the tangential bending stress  $\sigma_{\phi}^b$

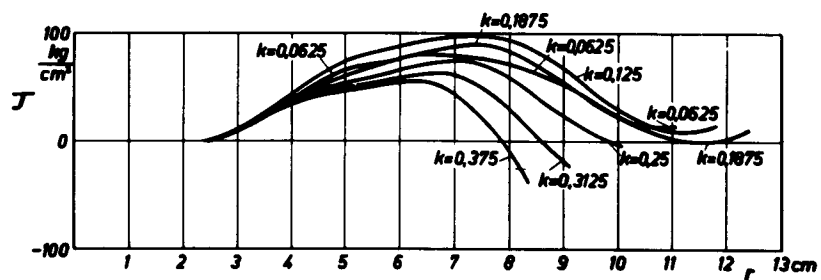
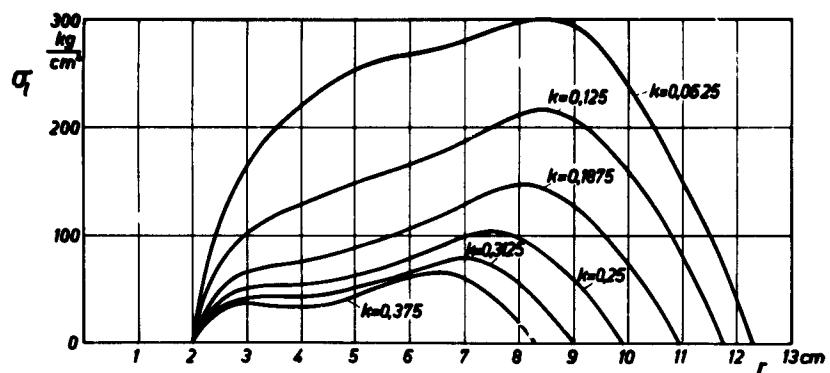


Fig. 21  
Analogous to Fig. 18, representation of the specified stresses  $\sigma_r$   
and  $\tau$



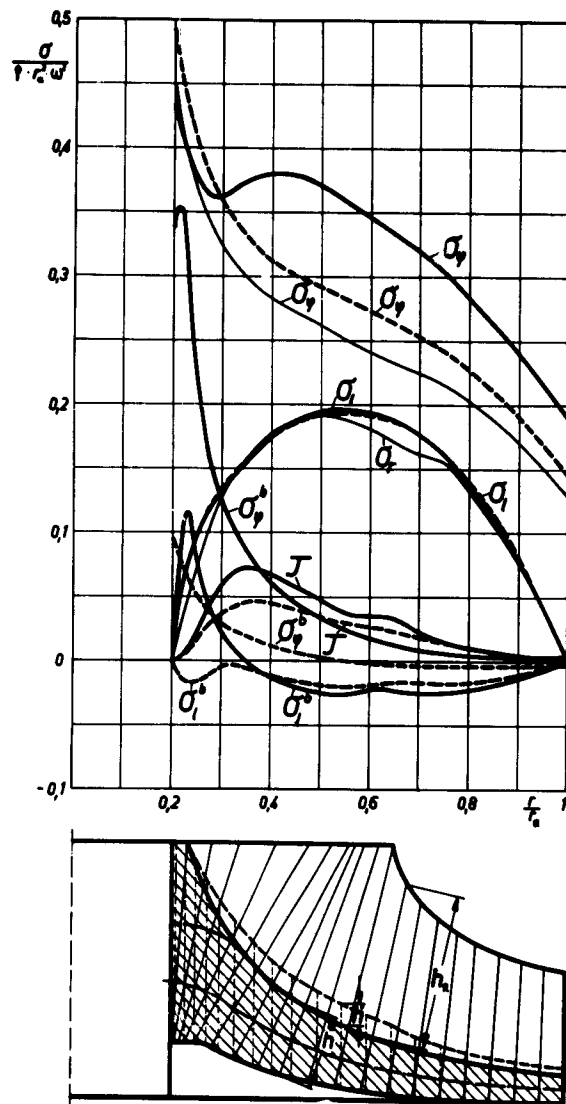


Fig. 22  
Calculated distribution of stresses in a model wheel  
with different designs of the rear of wheel body

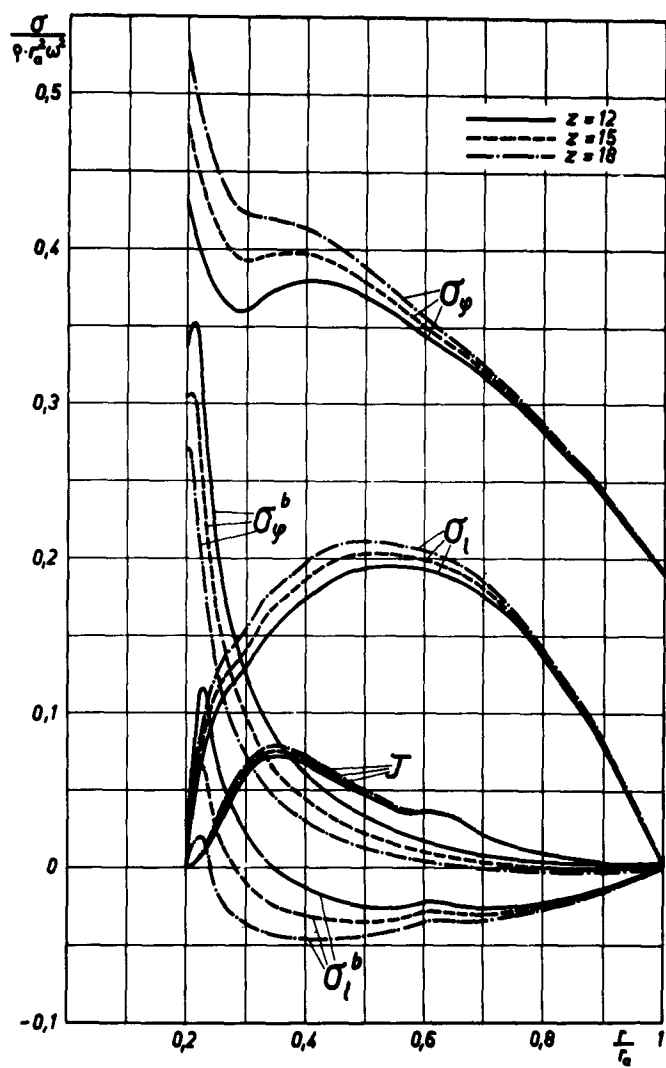


Fig. 23  
Influence of different blade numbers on the distribution  
of stresses in an impeller wheel

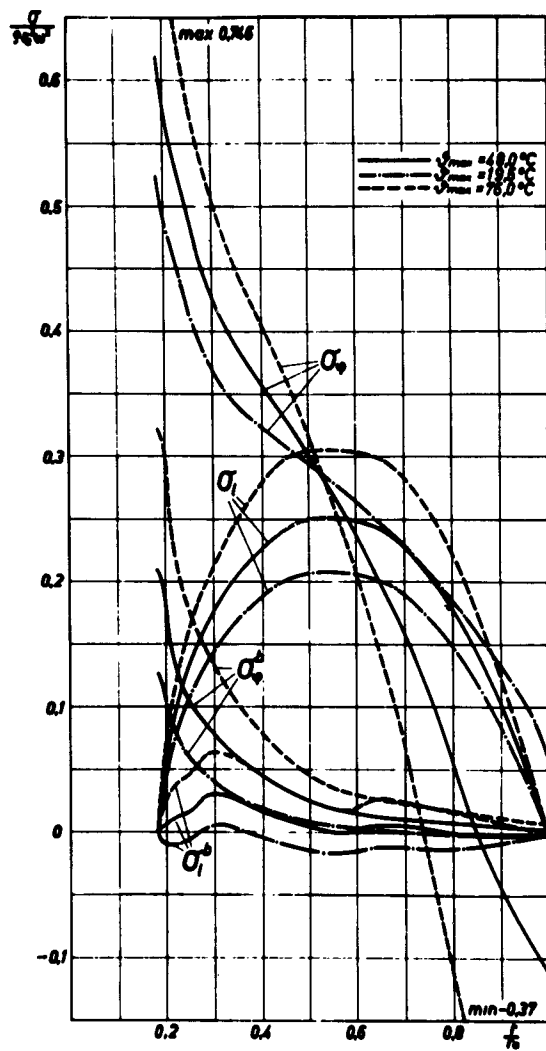
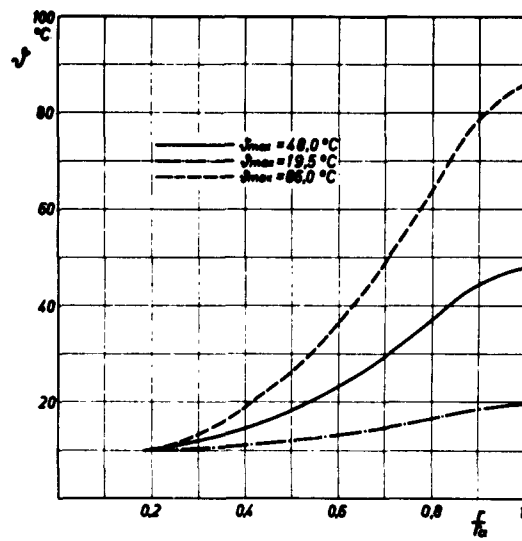
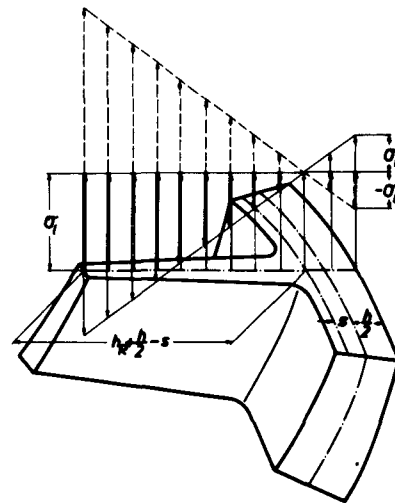


Fig. 24  
Influence of temperature fields on the stress  
fields of an impeller wheel



**Fig. 25**  
Representation of assumed temperature fields with regard to the distribution of stresses according to Fig. 24



**Fig. 26**  
Superposition of the normal stress  $\sigma_l$  with the bending stress  $\sigma_l^b$  on a finned shell element

ASD-TDR-62-1013

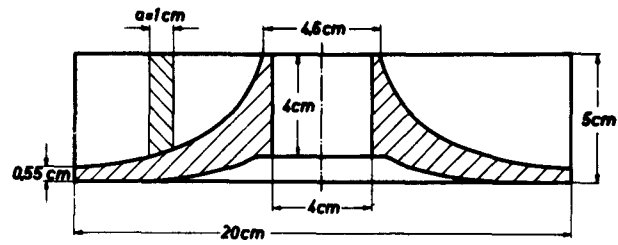


Fig. 27  
Representation of the first model wheel with the principal main dimensions

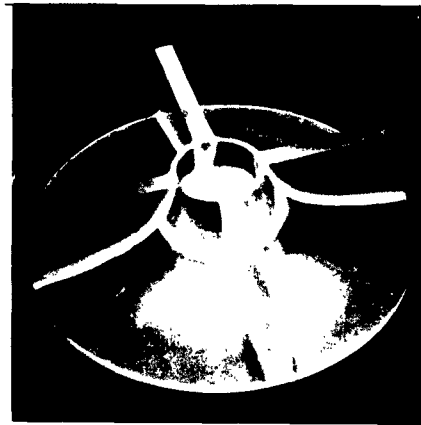


Fig. 28  
Illustration of the first built model wheel with four blades

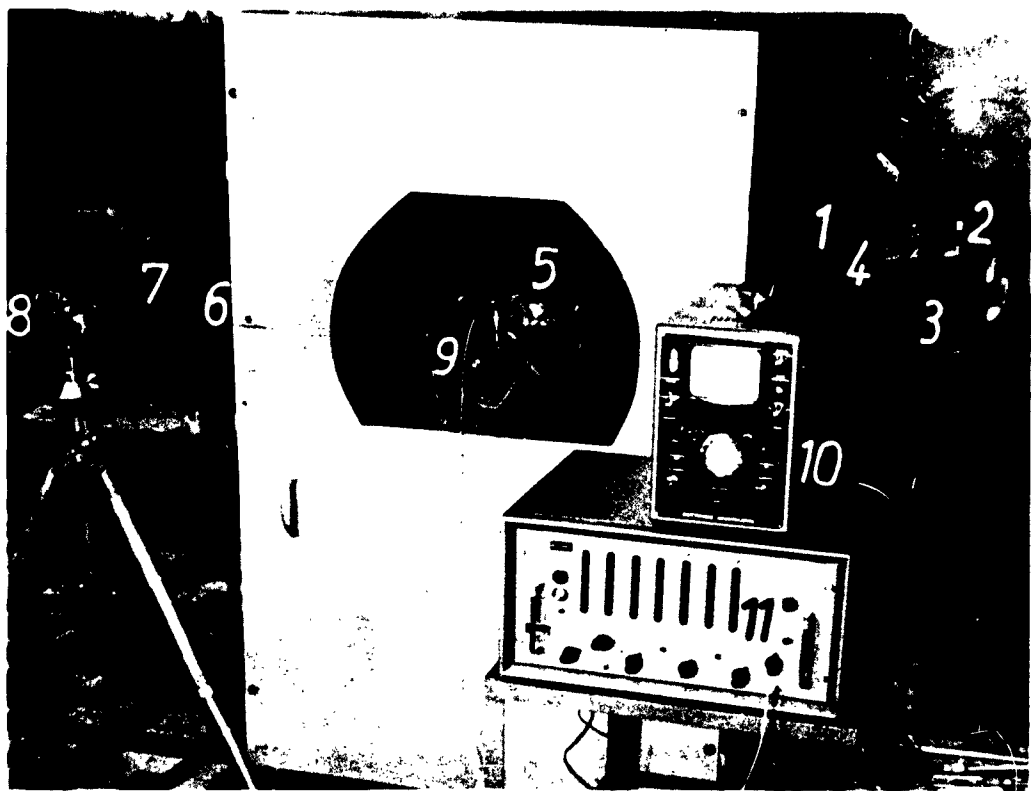


Fig. 29 a  
General view of the test stand with model and measuring equipment

- 1) stroboscope, apparatus for current supply and control unit
- 2) flash lamp
- 3) reflector between lamp and model
- 4) polarizer
- 5) model
- 6) analyzer
- 7) reflector between model and camera
- 8) camera
- 9) rotational transmitter
- 10) carrier frequency bridge for strain gage measurement
- 11) digital speed counter

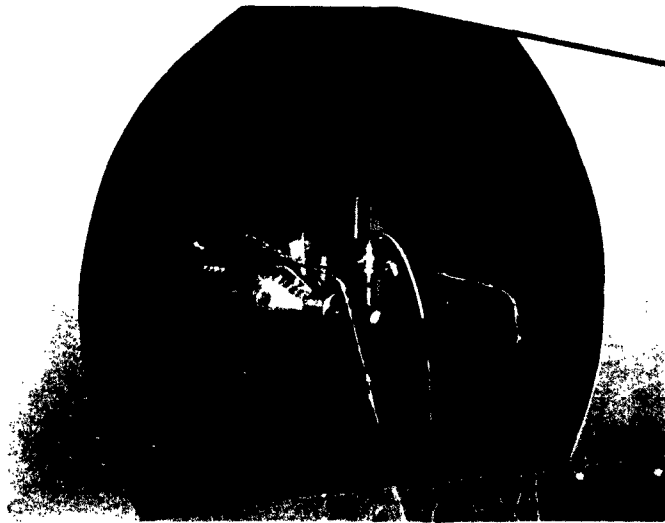


Fig. 29 b  
View of the mounted model disc in the test bed

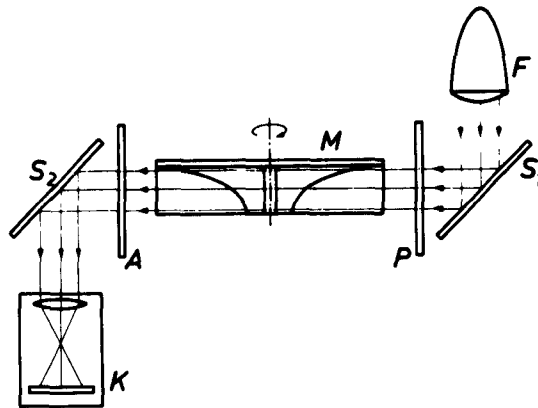


Fig. 30  
Representation of the way of light in a stroboscopic transillumination of the blades

F	flash lamp	M	model
S <sub>1</sub>	mirror	A	analyzer
S <sub>2</sub>	mirror	K	camera
P	polarizer		

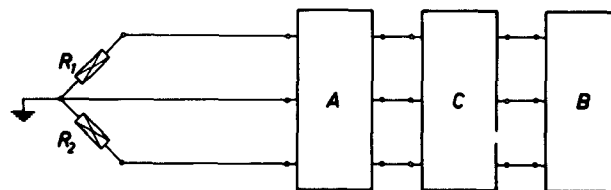


Fig. 31  
Measuring scheme for strain gage measuring

R <sub>1</sub>	active strain gage	B	carrier frequency measurement bridge
R <sub>2</sub>	compensator	C	switch for different strain gages
A	rotational transmitter		



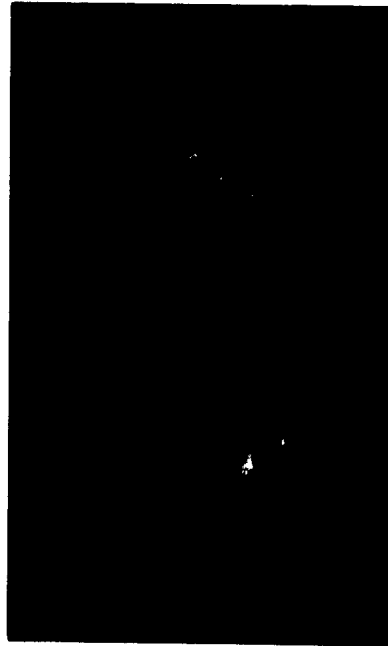
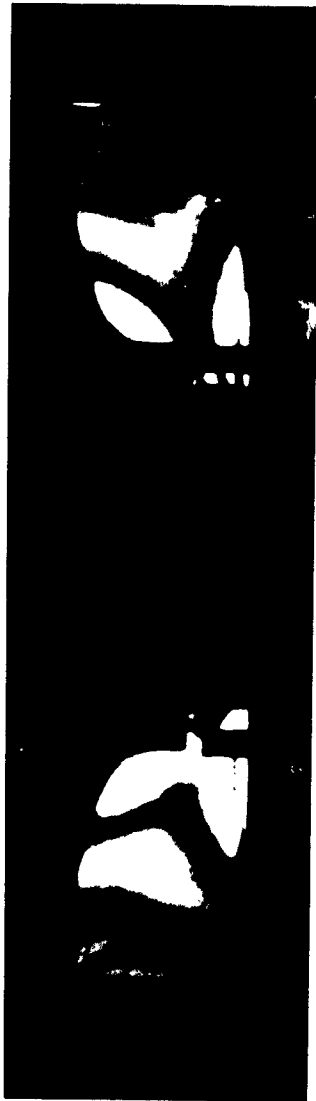


Fig. 32  
Fringe pattern photos of blades of the model wheel  
at a speed of  $n = 6000$  rpm

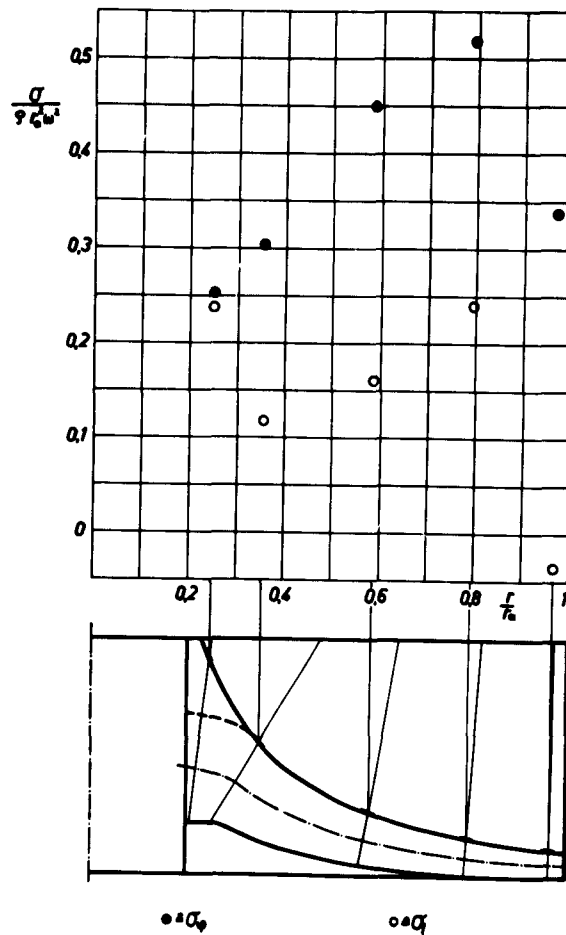


Fig. 33  
Stresses determined in the symmetric section  
between two blades by means of strain gages

Aeronautical Systems Division, Dir/Materials  
and Processes, Metals & Ceramics Lab, Wright-  
Patterson AFB, Ohio.  
Rpt Nr ASD-TDR-62-1013. INVESTIGATION OF THE  
GENERAL STRESS DISTRIBUTION IN IMPELLER  
WHEELS. Final report, Mar 63. 62p. incl  
illus., 39 refs.      Unclassified Report

This report contains a detailed illustration  
of new calculation data for impeller wheels.  
They are designed to furnish comparative  
figures for experimental investigations with  
systematically varied impeller wheels.  
Furthermore, initial experimental results  
are presented on the distribution of stresses

( over )

in a model of an impeller wheel.

1. Impellers
2. Stresses
3. Calculation data
- I. AFSC Project 7351  
Task 73521
- II. Contract AF 61  
(052)-520
- III. Technische Hochschule, Aachen, Germany
- IV. Prof. Dr.-Ing.  
Wilhelm Detmering  
Dip.-Ing. Wilhelm  
Soetebeer
- V. Secondary Rpt No.  
1 AD
- VI. Aval fr OTS
- VII. In ASTIA collection

Aeronautical Systems Division, Dir/Materials  
and Processes, Metals & Ceramics Lab, Wright-  
Patterson AFB, Ohio.  
Rpt Nr ASD-TDR-62-1013. INVESTIGATION OF THE  
GENERAL STRESS DISTRIBUTION IN IMPELLER  
WHEELS. Final report, Mar 63. 62p. incl  
illus., 39 refs.      Unclassified Report

This report contains a detailed illustration  
of new calculation data for impeller wheels.  
They are designed to furnish comparative  
figures for experimental investigations with  
systematically varied impeller wheels.  
Furthermore, initial experimental results  
are presented on the distribution of stresses

( over )

in a model of an impeller wheel.

1. Impellers
2. Stresses
3. Calculation data
- I. AFSC Project 7351  
Task 73521
- II. Contract AF 61  
(052)-520
- III. Technische Hochschule, Aachen, Germany
- IV. Prof. Dr.-Ing.  
Wilhelm Detmering  
Dip.-Ing. Wilhelm  
Soetebeer
- V. Secondary Rpt No.  
1 AD
- VI. Aval fr OTS
- VII. In ASTIA collection